

Chapter 4 1

Porous Copper Electrodes Formed 2

by the Constant and the Periodically 3

Changing Regimes of Electrolysis 4

Nebojša D. Nikolić 5 AU1

4.1 Introduction 6

The formation of open and porous structures with extremely large 7
surface area is of high technological significance, because this struc- 8
ture type is very suitable for electrodes in many electrochemical 9
devices, such as fuel cells, batteries and sensors [1, 2], and in cataly- 10
sis applications [3]. The template-directed synthesis method is most 11
commonly used for the preparation of such electrodes. This method 12
is based on a deposition of desired materials in interstitial spaces 13
of disposable hard template. When interstitial spaces of template are 14
filled by deposited material, the template is removed by combustion 15
or etching, and then the deposited material with the replica structure 16
of the template is obtained [4, 5]. The most often used hard templates 17
are porous polycarbonate membranes [6, 7], anodic alumina mem- 18
brane [8–10], colloidal crystals [11, 12], echinoid skeletal structures 19
[13], and polystyrene spheres [14, 15]. 20

N.D. Nikolić (✉)
ICTM-Institute of Electrochemistry, University of Belgrade,
Njegoseva 12, P.O.B. 473,11001 Belgrade, Serbia
e-mail: nnikolic@tmf.bg.ac.rs

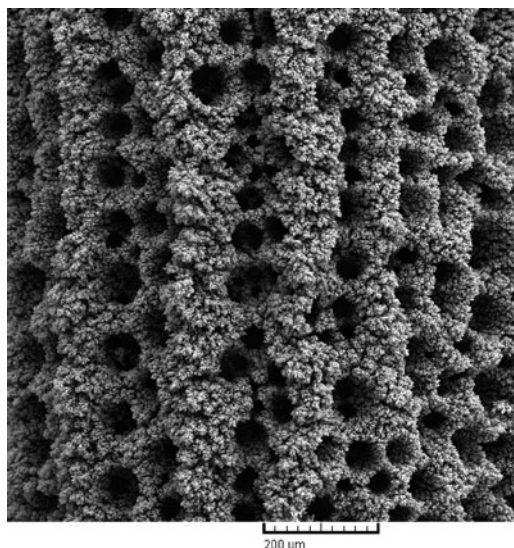


Fig. 4.1 The honeycomb-like structure formed by electrodeposition from 0.15 M CuSO_4 in 1.0 M H_2SO_4 at an overpotential of 1,000 mV with a quantity of the electricity 10 mAh/cm^2 (Reprinted from [22] with permission from Elsevier and [23] with permission from Springer.)

21 Electrodeposition technique showed as very favorable way for the
22 production of porous electrodes [1, 2, 4]. The open porous copper and
23 copper-tin alloys electrodes, denoted as both 3-D foam [1, 2, 4]
24 and honeycomb-like ones [16–23], are formed by electrodeposition
25 at high current densities and overpotentials, where parallel to
26 electrodeposition process, the hydrogen evolution reaction occurs.
27 The main characteristics of these electrodes are holes or pores formed
28 by attached hydrogen bubbles surrounded by metals grain agglom-
29 erates or dendritic particles (Fig. 4.1). This way of preparing porous
30 electrodes is denoted as gas bubble dynamic template method, where
31 the hydrogen bubbles function as a dynamic template for the forma-
32 tion of this type of deposits. The advantage of producing porous
33 materials by this hydrogen bubble dynamic template method when
34 compared with hard template methods is its low cost, ease of prepa-
35 ration, facile control of structure, and facile one-step synthesis
36 process, including preparation of the template, metal deposition,
37 and elimination of the template [5].

4.2 Potentiostatic Regime of Electrolysis 38

In potentiostatic regimes of electrolysis, honeycomb-like copper electrodes are formed by electrochemical deposition at overpotentials outside the plateau of the limiting diffusion current density where the parallelism between copper electrodeposition rate and hydrogen evolution reaction is evident [16, 23]. Hydrogen evolution responsible for the formation of the honeycomb-like electrodes was vigorous enough to cause such stirring of the copper solution which leads to the decrease of the cathode diffusion layer thickness and to the increase of the limiting diffusion current density and hence to the change of the hydrodynamic conditions in the near-electrode layer [16]. For copper solutions containing 0.15 M CuSO_4 and less (in 0.50 M H_2SO_4), the critical quantity of evolved hydrogen leading to a change of hydrodynamic conditions in the near-electrode layer was estimated to correspond to the average current efficiency of hydrogen evolution of 10.0% [20].

4.2.1 Phenomenology of Formation of the Honeycomb-Like Structures 54

The formation of porous deposits by dynamic template method can be briefly presented as follows: in the initial stage of the electrodeposition process, both the nuclei of deposited metal and the “nuclei” of hydrogen bubbles are formed at the active sites of the electrode surface (Fig. 4.2a) [18]. The hydrogen bubbles isolate the substrate and then the current lines are concentrated around them making rings consisted of agglomerates of grains of deposited metal. The current lines are also concentrated at the metal nuclei formed in the initial stage between the hydrogen bubbles forming copper grains agglomerates of them. In the growth process, due to current density distribution effect, both hydrogen evolution and copper nucleation primarily occur at top of these agglomerates. Some of the new, freshly formed hydrogen bubbles will coalesce with hydrogen bubbles formed in the initial stage of electrodeposition process, leading to their growth with

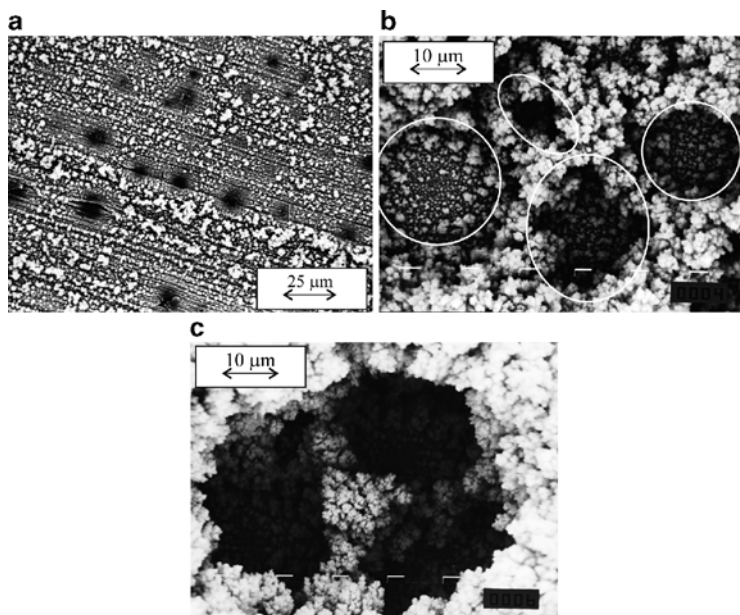


Fig. 4.2 Copper deposits electrodeposited from 0.15 M CuSO_4 in 0.50 M H_2SO_4 at an overpotential of 1,000 mV. Time of electrolysis: (a) 10 s; (b) 30 s, and (c) 120 s (Reprinted from [18, 23] with permission from Springer.)

70 electrolysis time. When the critical size of these hydrogen bubbles
71 to detach from electrode surface is reached, they will detach from
72 electrode surface forming holes of regular shapes at electrode
73 surface. This “regular” type of holes is shown in Fig. 4.2b in circle.
74 Simultaneously, holes of irregular shape are formed at electrode
75 surface of agglomerate copper grains formed between hydrogen
76 bubbles [18]. These “irregular” holes are situated between regular
77 holes, and they are shown in Fig. 4.2b in ellipse. For longer electro-
78 deposition time, coalescence of closely formed hydrogen bubbles
79 occurs, leading to the formation of large so-called coalesced holes
80 (Fig. 4.2c) [18].

81 Meanwhile, some of the new, freshly formed hydrogen bubbles will
82 not coalesce with the previously formed hydrogen bubbles because

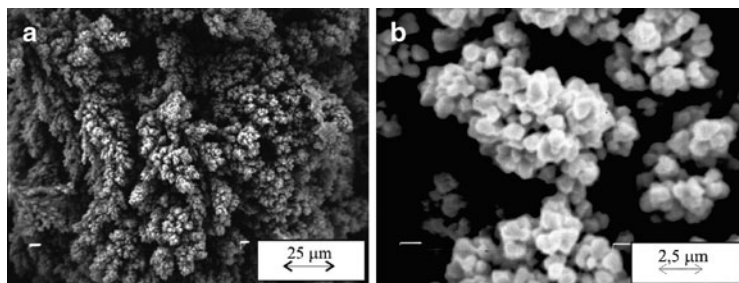


Fig. 4.3 Copper deposits electrodeposited from 0.075 M CuSO_4 in 0.50 M H_2SO_4 at an overpotential of 1,000 mV. Quantity of electricity: 20 mAh/cm² (Reprinted from [19] with permission from Elsevier and [23] with permission from Springer.)

they are situated between the freshly formed copper nucleus and 83
these hydrogen bubbles have not enough place to develop in large 84
hydrogen bubbles. These hydrogen bubbles will detach very fast 85
from the electrode surface forming a channel structure through the 86
interior of the deposit [19]. The typical channel structure formed by 87
simultaneous hydrogen evolution and copper nucleation is shown in 88
Fig. 4.3a. The “top view” of the part of the honeycomb-like struc- 89
ture shown in Fig. 4.3a is given in Fig. 4.3b; from it can be seen 90
cauliflower-like agglomerates of copper grains surrounded by irreg- 91
ular channels for which the origin is of evolved hydrogen. 92

All elements constructing the honeycomb-like structure can 93
also be seen from Fig. 4.4 showing a cross-section of this type of 94
deposit [24]. 95

The “regular holes” formed by both the attached hydrogen 96
bubbles (part in circle denoted with *A* in Fig. 4.4a) and the coales- 97
cence of neighboring hydrogen bubbles (part in circle denoted with *B* 98
in Fig. 4.4a) and “irregular holes” formed due to the effect of current 99
distribution at the growing surface (parts denoted by arrow labeled *C* 100
in Fig. 4.4a) are shown in Fig. 4.4a [24]. The presence of channel 101
structures formed through the interior of the deposit can be easily 102
observed by cross-section analysis of this deposit at a higher magni- 103
fication (Fig. 4.4b). 104

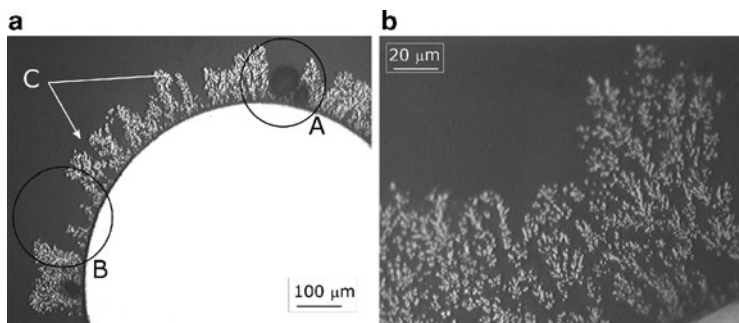


Fig. 4.4 Cross section of copper deposit electrodeposited from 0.15 M CuSO_4 in 0.50 M H_2SO_4 , at an overpotential of 1,000 mV with a quantity of the electricity of 10 mAh/cm^2 (Reprinted from [24] with permission from Serbian Chemical Society.)

105 **4.2.2 Parameters Affecting Number, Size**
 106 **and Distribution of Holes in the**
 107 **Honeycomb-Like Structures**

108 Electrodeposition technique is a suitable way to get open and porous
 109 structure because it is very easy to control number, size and distribution
 110 of holes by the choice of appropriate electrodeposition conditions [19].

111 Factors affecting number, size, and distribution of holes are:

- 112 (a) Overpotential of electrodeposition
- 113 (b) Preparation of working electrode
- 114 (c) Concentration of Cu(II) ions
- 115 (d) Concentration of sulfuric acid
- 116 (e) Temperature of electrolysis
- 117 (f) Time of electrolysis

118 **4.2.2.1 Overpotential of Electrodeposition**

119 Increasing the overpotential intensifies hydrogen evolution reaction [16,
 120 23]. For copper solution containing 0.15 M CuSO_4 in 0.50 M H_2SO_4 , the
 121 average current efficiency of hydrogen evolution, $\eta_{I,av}(\text{H}_2)$, was about
 122 three times larger at an overpotential of 1,000 mV ($\eta_{I,av}(\text{H}_2) = 30.0\%$)
 123 than at 800 mV ($\eta_{I,av}(\text{H}_2) = 10.8\%$) [16]. It is manifested by the

formation of the honeycomb-like structures with the considerably larger number of holes formed of detached hydrogen bubbles at 1,000 mV than at 800 mV.

4.2.2.2 Preparation of Working Electrode

The number, size, and distribution of holes in the honeycomb-like electrodes strongly depended on the type of working electrode used for copper electrodeposition [17, 18]. The strong difference in the initial stage of their formation, as well as in the formed honeycomb-like structures, was observed in the dependence of the type of used working electrode. The number of hydrogen bubbles formed at the electrode with large number of active centers, where irregularities at electrode surface represent active centers for the formation of both the hydrogen bubbles and agglomerates of copper grains, was several times higher than the number of holes formed at the electrode with “killed” active centers, where active centers were removed by the formation of uniform thin copper film by electrodeposition at some lower overpotential [18].

4.2.2.3 Concentration of Cu(II) Ions

The increase of concentration of Cu(II) ions causes a sharp decrease of the quantity of evolved hydrogen and hence the decrease of the average current efficiencies for hydrogen evolution reaction [19, 20], what is in a good agreement with the prediction of the ionic equilibrium of the species in the $\text{CuSO}_4\text{-H}_2\text{SO}_4\text{-H}_2\text{O}$ system [21, 25, 26]. Electrodeposition processes from copper solutions containing the concentration of Cu(II) ions above 0.15 M CuSO_4 (in 0.50 M H_2SO_4) lead to the formation of new type of holes, denoted as dish-like hole [19]. The typical dish-like holes obtained by electrodeposition from 0.60 M CuSO_4 in 0.50 M H_2SO_4 at an overpotential of 1,000 mV are shown in Fig. 4.5a. The appearance of very branchy dendrites between dish-like holes (Fig. 4.5b), and at shoulders of holes with longer electrodeposition times (Fig. 4.5c) clearly points out that the diffusion layer of the macroelectrode is not disturbed during copper electrodeposition from this solution, and that the quantity of evolved hydrogen

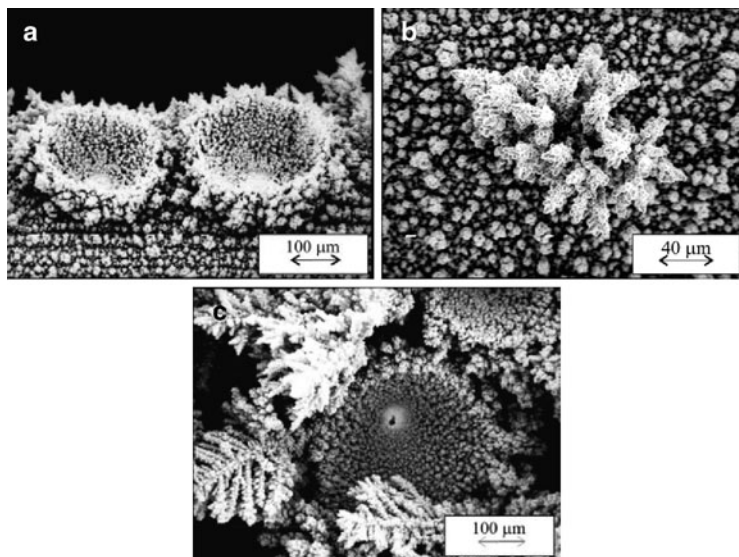


Fig. 4.5 Copper deposits electrodeposited from 0.60 M CuSO_4 in 0.50 M H_2SO_4 at an overpotential of 1,000 mV. Quantity of electricity: (a) and (b) 2.5 mAh/cm^2 and (c) 20 mAh/cm^2 (Reprinted from [19] with permission from Elsevier and [23] with permission from Springer.)

157 was not enough to cause stirring of solution in the near-electrode layer.
158 Honeycomb-like structures were formed during copper electrodeposition
159 from solutions with concentrations of Cu(II) ions less than 0.15 M
160 CuSO_4 (for example, from 0.075 M CuSO_4 in 0.50 M H_2SO_4) [19].

161 The concentration of 0.30 M CuSO_4 (in 0.50 M H_2SO_4) is the
162 transitional concentration between lower and higher concentrations
163 of Cu(II) ions. The mixture of holes forming the honeycomb-like
164 structure and dish-like holes was obtained by electrodeposition from
165 this solution at an overpotential of 1,000 mV (Fig. 4.6) [19].

166 4.2.2.4 Concentration of Sulfuric Acid

167 The effect of H_2SO_4 on copper electrodeposition processes was
168 examined keeping the concentration of Cu(II) ions constant

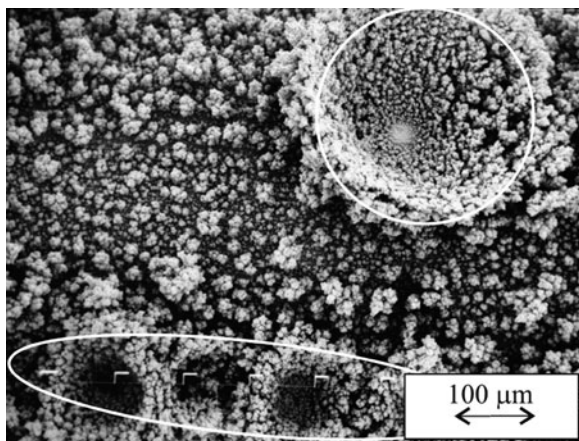


Fig. 4.6 Copper deposit obtained at an overpotential of 1,000 mV from 0.30 M CuSO_4 in 0.50 M H_2SO_4 with a quantity of the electricity of 2.5 mAh/cm² (Reprinted from [19] with permission from Elsevier and [23] with permission from Springer.)

(0.15 M CuSO_4), while the concentration of H_2SO_4 was varied, and they were 0.125, 0.25, and 1.0 M H_2SO_4 [22]. As expected, the increasing H_2SO_4 concentration led to the increase of the average current efficiencies of hydrogen evolution. The main characteristics of electrodeposition processes at an overpotential of 1,000 mV from the solutions containing 0.15 M CuSO_4 in both 0.25 and 1.0 M H_2SO_4 were holes or pores surrounded by agglomerates of copper grains. Aside from holes and cauliflower-like agglomerates of copper grains between them, degenerate dendrites, a channel structure around dendritic and cauliflower-like particles and holes with the shoulders of degenerate dendrites were electrodeposited at 1,000 mV from 0.15 M CuSO_4 in 0.125 M H_2SO_4 [22, 23]. These morphological forms were obtained in spite of relatively high average current efficiency of hydrogen evolution of 20.3% by which this deposit was formed, and their formation can be explained by the effect of a density and a surface tension of the electroplating solution on the bubble break-off diameter [22, 23]. The number of holes increased with the increasing H_2SO_4 concentration, while the hole size decreased with the increasing H_2SO_4 concentration. Also, the

188 orientation of holes was changed from random oriented holes to holes
189 which were lined up in parallel rows [22].

190 4.2.2.5 Temperature of Electrolysis

191 The increase of temperature of electrolysis leads to an intensification
192 of hydrogen evolution reaction [27]. Meanwhile, despite intensifica-
193 tion of hydrogen evolution with the increasing temperature, the
194 decrease of the number of holes formed per mm^2 surface area of
195 electrodes and the increase of their average diameter were observed
196 during copper electrodeposition at an overpotential of 800 mV
197 (Fig. 4.7). To explain this unexpected trend in the development of
198 morphology of electrodeposited copper, the effect of temperature on
199 some properties of electroplating solution, such as viscosity and
200 surface tension, is considered [27]. The increase of temperature
201 causes the decrease of both the viscosity [28] and the surface tension
202 of this solution [29]. The decrease of the surface tension of the
203 solution lowers the break-off diameter of the hydrogen bubble from
204 the electrode surface [29], while the decreased viscosity of the
205 solution probably facilitates a transport of the detached hydrogen
206 bubbles through the interior of the deposit forming the channel
207 structure through it. Anyway, increasing temperature leads to
208 redistribution of evolved hydrogen from those creating honeycomb-
209 like structure (Fig. 4.7a, b) to structure with dish-like holes
210 (Fig. 4.7c) and by the dominant presence of agglomerates of copper
211 grains surrounded by irregular channels of evolved hydrogen (that is
212 a channel structure) (Fig. 4.7d).

213 4.2.2.6 Time of Electrolysis

214 The size of holes increases with electrolysis time due to the growth of
215 the hydrogen bubbles with time, as well as due to a coalescence of
216 neighboring hydrogen bubbles. In the growth process, due to the
217 current density distribution effect, some hydrogen bubbles can remain
218 captive in the interior of deposit making the honeycomb-like structure
219 very porous (Fig. 4.8; part in circle denoted with D) [24].

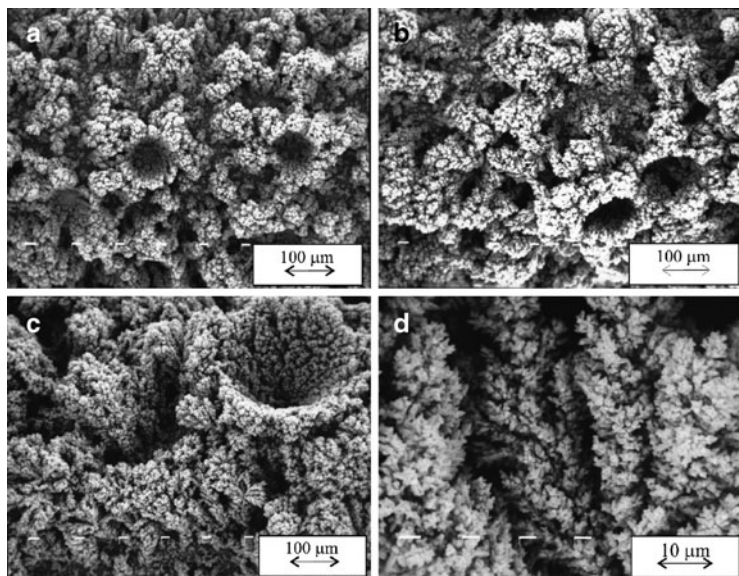


Fig. 4.7 Copper deposits electrodeposited at an overpotential of 800 mV from 0.15 M CuSO_4 in 0.50 M H_2SO_4 at temperatures of: (a) 14.0; (b) 35.0; (c) and (d) $50.0 \pm 0.5^\circ\text{C}$. Quantity of electricity: 10 mAh/cm^2 (Reprinted from [27] with permission from Serbian Chemical Society and [23] with permission from Springer.)

4.3 Galvanostatic Regime of Electrolysis

220

In galvanostatic regimes of electrolysis, the honeycomb-like 221
structures are formed at current densities larger than the limiting 222
diffusion current density [30]. The typical honeycomb-like 223
structure electrodeposited at a current density of 0.44 A/cm^2 , which is about 224
27.5 larger than the limiting diffusion current density, is shown in 225
Fig. 4.9a. From Fig. 4.9b–d, all elements of which this structure type 226
is constructed can be seen: individual hole formed by attached 227
hydrogen bubble (this type of hole is denoted as noncoalesced hole 228
in the future text; Fig. 4.9b), hole formed by coalescence of closely 229
formed hydrogen bubbles (this type of hole is denoted as coalesced 230

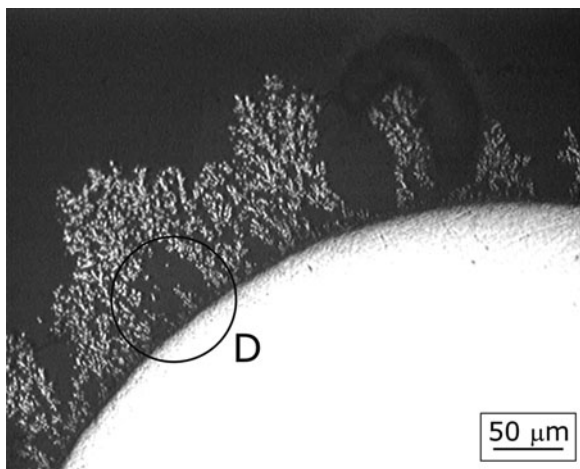


Fig. 4.8 Cross section of copper deposit electrodeposited from 0.15 M CuSO_4 in 0.50 M H_2SO_4 at an overpotential of 1,000 mV with a quantity of the electricity of 10 mAh/cm^2 (Reprinted from [24] with permission from Serbian Chemical Society.)

231 hole in the future text; Fig. 4.9c), and cauliflower-like agglomerates
232 of copper grains formed around holes (Fig. 4.9d).

233 The hole size decreases while the number of holes increases with
234 the increasing current density of electrodeposition [5].

235 4.4 A Brief Review of Previous Results

236 The increasing overpotential, the decreasing concentration of Cu(II)
237 ions, and the increasing H_2SO_4 concentration intensify the hydrogen
238 evolution reaction. The intensification of hydrogen evolution leads to
239 an increase of the number of formed holes, as well as to a decrease of
240 hole size. Meanwhile, the ratio of the coalesced holes to the overall
241 number of formed holes increased with the intensification of hydro-
242 gen evolution.

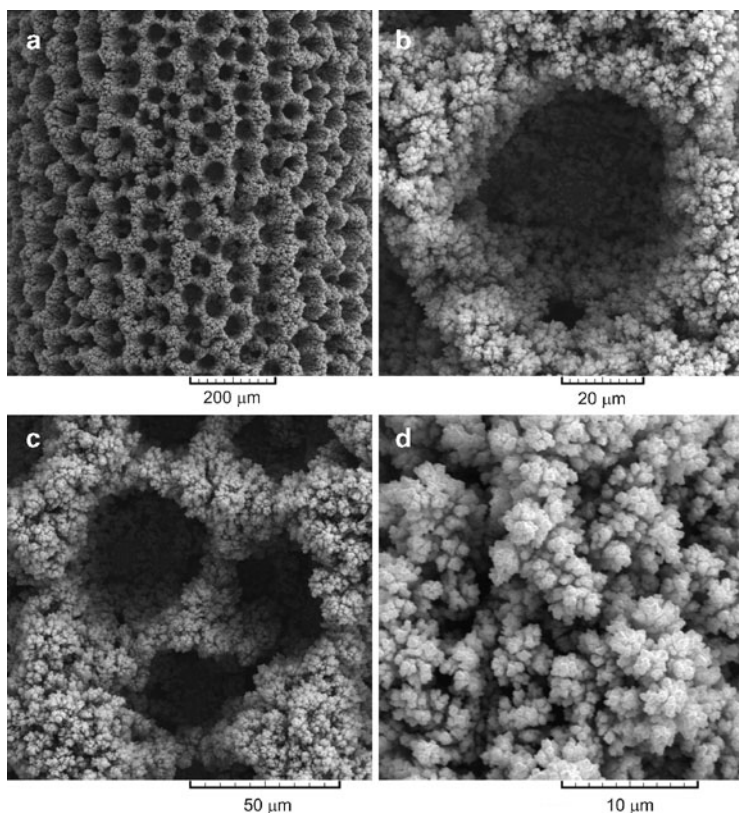


Fig. 4.9 (a) The honeycomb-like structure formed at a current density of 0.44 A/cm^2 and the typical elements constructing this type of structure; (b) noncoalesced hole; (c) coalesced hole; and (d) cauliflower-like agglomerates of copper grains formed around holes (Reprinted from [30] with permission from Elsevier.)

The process of a coalescence of closely formed hydrogen bubbles 243
should be avoided during the formation of the honeycomb-like 244
deposits because this process causes both the decrease of the overall 245
number of the formed holes and the increase of the hole size and 246
hence leads to the decrease of the specific surface area of these 247
electrodes. 248

249 To increase the specific surface area and enhance the effectiveness/
250 activity of the porous electrodes, it is necessary to reduce the size of
251 the pores, as well as the branches in the foam or agglomerates of
252 copper grains in the honeycomb-like structures [4].

253 The two ways are proposed to increase the specific surface area of
254 open porous copper electrodes and to improve micro- and
255 nanostructural characteristics of these electrodes. The first way is
256 the addition of specific substances, known as additives, to the
257 electroplating solution [4]. So, the decrease of the diameter of holes,
258 as well as the increase of their number in 3D foam copper structures,
259 can be realized by the addition of acetic acid to the copper sulfate
260 solution [4]. Also, the addition of chloride ions dramatically reduces
261 the size of the copper branches in the walls of holes. The reduction in
262 pore size is a result of lowering hydrophobic force of the generated
263 hydrogen gas by adding bubble stabilizer (e.g., acetic acid) that
264 suppresses the coalescence of bubbles, while the decrease in branch
265 size in the foam wall is a consequence of the catalytic effect of
266 chloride ions on the copper deposition reaction. Mechanical strength
267 of the foam structure can be improved by the addition of $(\text{NH}_4)^+$, Cl^- ,
268 polyethylene glycol, and 3-mercapto-1-propane sulfonic acid to the
269 deposition bath [31]. The foam structure obtained by a combination of
270 these additives was a highly porous with better mechanical strength
271 than the one obtained without additives, owing to higher compactness
272 of crystallites. Meanwhile, the use of additives in electroplating
273 practice leads to their consumption during electrodeposition pro-
274 cesses and the requirement for their permanent control is necessary.
275 The consumption of additives occurs due to removal with the plated
276 objects, by their incorporation in the deposit (codeposition) and by
277 reaction on the plated object [32, 33].

278 The second way for the increase of the specific surface area of
279 copper electrodes is the application of periodically changing regimes
280 of electrolysis, such as pulsating overpotential (PO), pulsating cur-
281 rent (PC), and reversing current (RC). The application of PO
282 regime is primarily important from academic point of view for
283 understanding mechanism of electrodeposition processes at periodi-
284 cally changing rate. For technological purposes, pulse and reverse
285 plating techniques, such as pulsating current (PC) and reversing
286 current (RC), are more important [34, 35].

4.5 The Regime of Pulsating Overpotential

287

Pulsating overpotential (PO) consists of a periodic repetition of overpotential pulses of different shapes [34, 35]. Square-wave PO is defined by the overpotential amplitude, η_A , deposition pulse, t_c , and pause, t_p . The pause to pulse ratio is defined as $p = t_p/t_c$.

4.5.1 Characteristics of the Honeycomb-Like Structures Obtained by the PO Regime and Their Comparison with Those Obtained by the Constant Regimes of Electrolysis

292

293

294

295

Figure 4.10 shows the honeycomb-like electrodes obtained at a constant overpotential of 1,000 mV (Fig. 4.10a) and by the PO regime with the overpotential amplitude of 1,000 mV, deposition pulse, t_c , of 10 ms, and pause duration, t_p , of 50 ms (Fig. 4.10b). The difference in the number of holes, as well as in their size, can be clearly seen from this figure. In all experiments for which results are presented in this section,

296

297

298

299

300

301

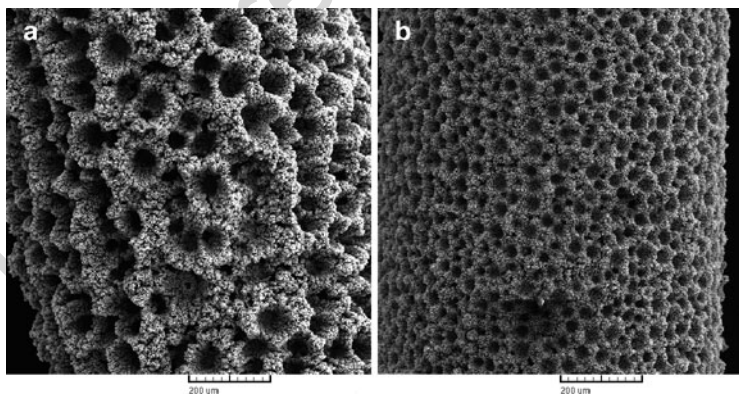


Fig. 4.10 Honeycomb-like structures obtained: (a) at a constant overpotential of 1,000 mV and (b) by PO regime with deposition pulse of 10 ms and a pause of 50 ms (Reprinted from [36] with permission from Elsevier.)

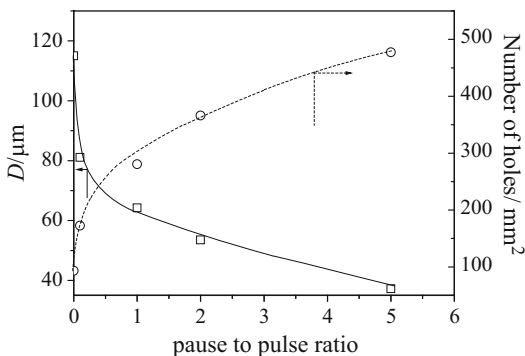


Fig. 4.11 The dependences of the average diameter of the surface holes, D , (*square*) and the number of holes per mm^2 surface area of the copper electrode (*circle*) on the pause to pulse ratio (Reprinted from [36] with permission from Elsevier.)

302 electrodeposition of copper was performed from 0.15 M CuSO_4 in
 303 0.50 M H_2SO_4 at room temperature using cylindrical copper electrodes
 304 [24, 36, 37]. In pulsating overpotential (PO) deposition the
 305 overpotential amplitude of 1,000 mV and pulse duration of 10 ms
 306 were applied. A pause duration was selected to be 5, 10, 20, 50, and
 307 100 ms (the pause to pulse ratios were 0.5, 1, 2, 5, and 10, respectively).

308 The dependences of the average diameter of the holes and of the
 309 number of holes formed per mm^2 surface area of the honeycomb-like
 310 copper electrodes on the pause to pulse ratio are shown in Fig. 4.11.

311 The decrease of the hole size and the increase of the number of
 312 formed holes with the increasing pause to pulse ratio can be primarily
 313 ascribed to the suppression of a coalescence of closely formed
 314 hydrogen bubbles [36]. The coalesced holes are observed in the
 315 honeycomb-like structures formed with pause to pulse ratios up to
 316 2. Holes formed with the pause durations shorter than the deposition
 317 pulse were similar to those obtained at constant overpotential [36].
 318 The bottom of these holes was very compact (Fig. 4.12a, b).
 319 The prolonging pause duration led to the change of the bottom of
 320 holes from compact to the one constructed of very disperse
 321 agglomerates of copper grains (Fig. 4.12c). The significantly smaller
 322 number of holes was formed with a pause duration of 100 ms and

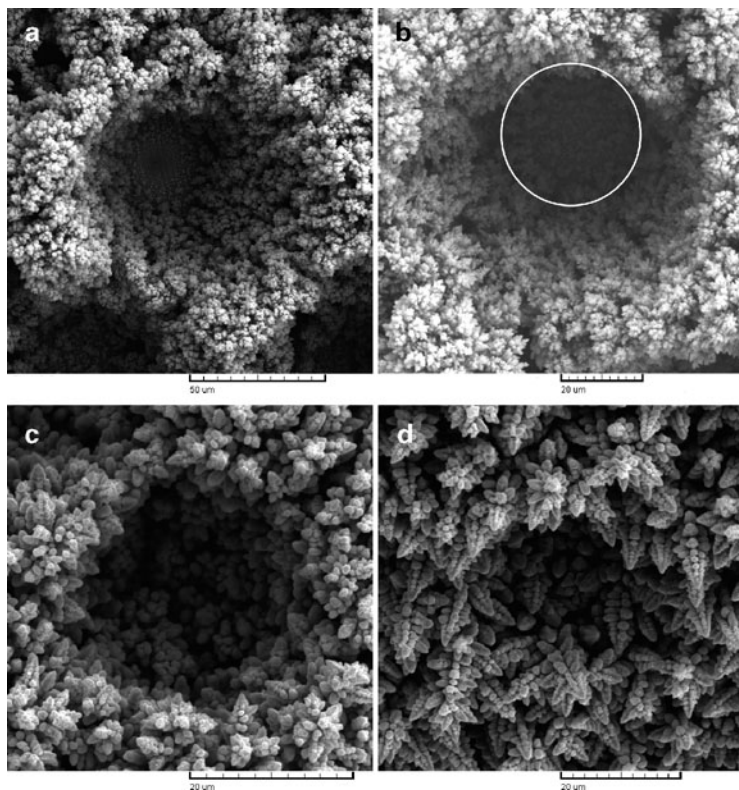


Fig. 4.12 Holes formed by attached hydrogen bubbles obtained at: (a) a constant overpotential of 1,000 mV and by PO regimes with a pause duration of: (b) 5 ms; (c) 50 ms; and (d) 100 ms. Deposition pulse: 10 ms (Reprinted from [36] with permission from Elsevier and [37] with permission from Springer.)

these holes were completely different from those obtained with the 323
smaller pause to pulse ratios [37]. This type of holes was constructed 324
from dendrites (Fig. 4.12d). 325

Simultaneously, the morphology of electrodeposited copper 326
formed around holes, as well as inside holes, changed with the 327
increasing pause to pulse ratio from cauliflower-like agglomerates 328
of copper grains to dendrites. Very disperse agglomerates of copper 329
grains were formed at the constant overpotential and by the PO 330

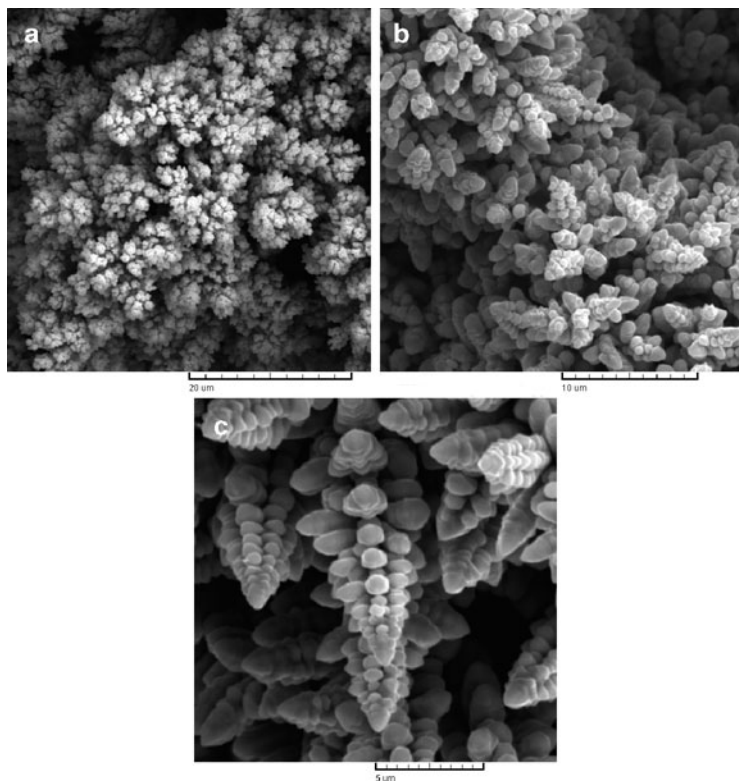


Fig. 4.13 Morphologies of electrodeposited copper formed around holes: (a) at a constant overpotential of 1,000 mV and by the PO regimes with pause duration of: (b) 50 ms and (c) 100 ms. Deposition pulse: 10 ms (Reprinted from [36, 38] with permission from Elsevier.)

331 regimes with pause durations shorter than the deposition pulse
332 (Fig. 4.13a). Copper dendrites are noticed at shoulders of holes
333 electrodeposited with pause duration of 20 ms and their number
334 and size increased with the prolonging pause durations, as
335 shown in Fig. 4.13b for the morphology of electrodeposited copper
336 obtained with a pause duration of 50 ms. Finally, the walls of holes
337 obtained with pause duration of 100 ms were only composed of
338 dendrites (Fig. 4.13c). The appearing of dendritic forms clearly

indicates a decrease of effectiveness of stirring of copper solution by evolved hydrogen with the increase of pause duration.

The analysis of the interior of holes obtained with pause durations up to 50 ms showed that the prolongation of pause duration leads to a reduction of the size of agglomerates of copper grains of which the walls of holes are constructed. With the prolonging pause duration up to 50 ms, holes became closer to each other, while compactness of the formed agglomerates between them was also increased [36]. The size of grains of which both cauliflower-like agglomerates and dendrites are composed increased with increasing pause to pulse ratio due to the selective dissolution of grains during the pauses. It was shown [39] that the smaller grains would dissolve faster than the larger ones due to the Kelvin effect [40]. In addition, the structure of the grains becomes more regular with increasing pause duration due to the fact that the adatoms in nonstable positions dissolve faster than the atoms in a stable position in lattice [35]. Finally, the deposit at the shoulders of the holes dissolve faster due to the edge effect, which also leads to the formation of a more homogenous distributed deposit with increasing pause duration and to an increased number of less deep holes.

The increased compactness of the copper deposits, the suppression of coalescence of neighboring hydrogen bubbles, and a decrease of the depth of the holes can be clearly seen from Fig. 4.14 showing cross section of copper deposits obtained with different pause to pulse ratios [24]. The compactness of the formed deposits increased with the increasing pause duration [24], and it was larger than the compactness of the deposit obtained by the constant regime of electrolysis (Fig. 4.4a). From Figs. 4.8 and 4.14, it can be seen that the increase of the number of holes by the application of PO regime can be ascribed not only to suppressed coalescence of neighboring hydrogen bubbles but also to the improved current distribution at growing copper surface by which an inclusion of hydrogen bubbles in deposit was prevented. Due to the current density distribution effect, the loosing of "irregular holes" was also observed by the application of PO regimes. With the prolonging pause duration, pores or channels formed through the interior of deposits were mutually coalesced forming larger pores. In this way, a transport of electroactive species through the interior of structures was facilitated, what is very desirable for evaluation of electrochemical reactions [1].

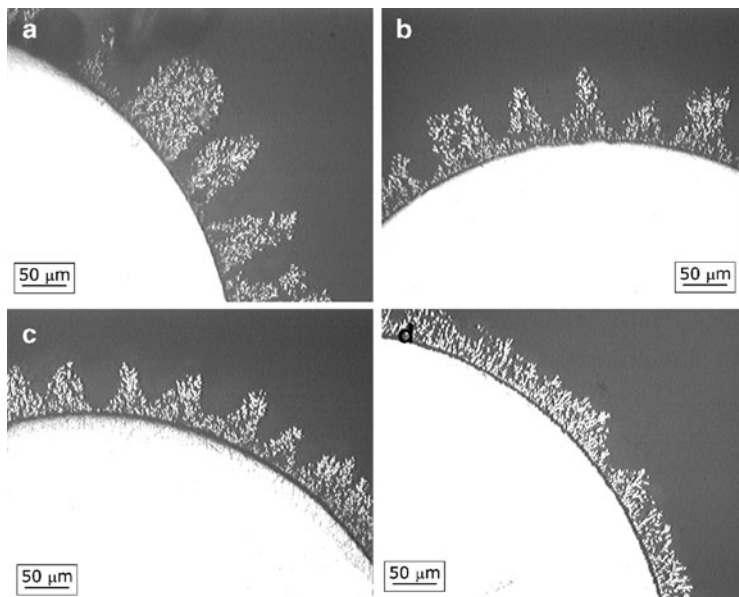


Fig. 4.14 Cross section of copper deposits electrodeposited by pulsating overpotential (PO) regime with pause duration of: (a) 5 ms; (b) 20 ms; (c) 50 ms; and (d) 100 ms. Deposition pulse: 10 ms (Reprinted from [24] with permission from Serbian Chemical Society.)

378 Anyway, the effects observed by the application of PO regime are
379 ascribed to a current density during “off” periods (i.e., during dura-
380 tion of pause). Although this current density can be neglected in
381 comparison with the current density during “on” periods (i.e., during
382 the duration of deposition pulse), it is clear that its effect on the
383 formation of these deposits is very important [36, 37].

384 **4.5.2 Formation of the Honeycomb-Like** 385 **Structures by the PO Regime**

386 The values of the average current efficiencies of hydrogen evolution,
387 $\eta_{I,av}(H_2)$, obtained for different pause to pulse ratios are given in
388 Table 4.1 [41]. The following parameters of square-waves PO were

Table 4.1 The values of the average current efficiencies of hydrogen evolution, $\eta_{l,av}(H_2)$, in %, obtained for different pause to pulse ratios (t_c deposition pulse; t_p pause duration)

$t_c:t_p$	1:10	3:10	5:10	10:10	20:10
$\eta_{l,av}(H_2)$ (%)	0	16.4	22.4	27.2	28.1

Reprinted from [41] with permission from Elsevier

analyzed: the overpotential amplitude of 1,000 mV, pause duration of 10 ms, and deposition pulses of 1, 3, 5, 10, and 20 ms.

The pyramid-like forms were electrodeposited by square-wave PO with a deposition pulse of 1 ms (Fig. 4.15a, b). These pyramid-like forms represent precursors of dendrites, what is concluded by the comparison with the top of copper dendrites obtained by copper electrodeposition at a constant overpotential of 650 mV (Fig. 4.15c). Copper pyramids of different shapes are also obtained by electrodeposition in a constant regime of electrolysis, where the morphology of pyramidal nanoparticles depended on the ratio of the concentration of surfactant/precursor and deposition time [42]. Despite the fact that the overpotential amplitude of 1,000 mV was used, holes for which the origin was of attached hydrogen bubbles were not formed (Fig. 4.15a). The absence of holes clearly indicates that a deposition pulse of 1 ms was insufficient for the formation of hydrogen bubbles.

From Fig. 4.16, it can be seen that honeycomb-like structures were formed with deposition pulses of 3, 5, 10, and 20 ms. The analysis of the honeycomb-like structures showed that the number of holes formed by the attached hydrogen bubbles did not change considerably with the length of deposition pulses of 3, 5, and 10 ms (i.e., with pause to pulse ratios up to 1). The mild decrease of the number of the formed holes was observed with a deposition pulse of 20 ms, what can be ascribed to the enhanced coalescence of neighboring hydrogen bubbles as well as to effects related to the current density distribution at the growing electrode by which some of the hydrogen bubbles remained captive in the interior of deposits [41].

Meanwhile, the strong effect of the length of deposition pulse on the morphology of electrodeposited copper formed around holes was achieved (Fig. 4.17). Copper dendrites were formed with a deposition

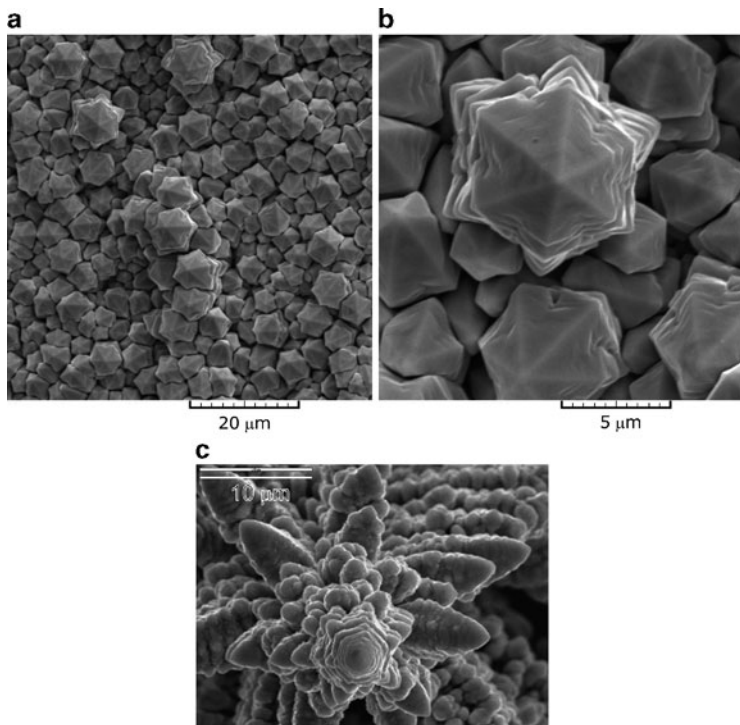


Fig. 4.15 (a) and (b) Pyramid-like precursors of dendrites obtained by square-wave PO with a deposition pulse of 1 ms and a pause of 10 ms; deposition time: 1,800 s, (c) top view of copper dendrite obtained by electrodeposition at an overpotential of 650 mV (Reprinted from [41] with permission from Elsevier.)

419 pulse of 3 ms (Fig. 4.17a). Although dendrites were also formed with
420 a deposition pulse of 5 ms (Fig. 4.17b), there were more branchy
421 structures than those obtained with a deposition pulse of 3 ms
422 (Fig. 4.17a). Agglomerates of copper grains were mainly formed
423 with a deposition pulse of 10 ms, while the presence of developed
424 dendrites was very rare (Fig. 4.17c). Finally, agglomerates of copper
425 grains were formed between holes when deposition pulse of 20 ms
426 was applied (Fig. 4.17d).

427 Figure 4.18 shows the cross section of the copper deposits obtained
428 with deposition pulses of 3, 5, 10, and 20 ms. Dendrites formed around

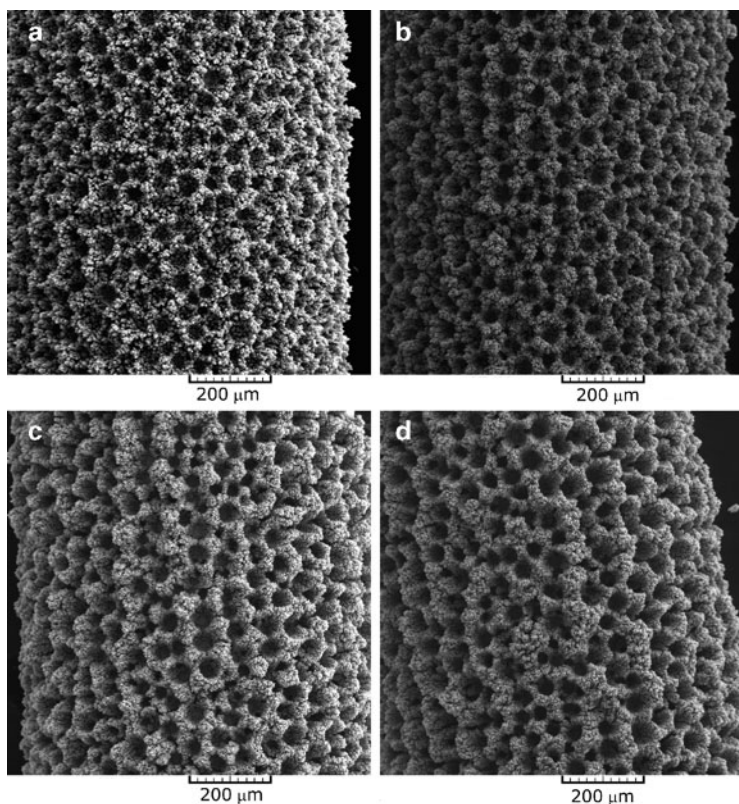


Fig. 4.16 Honeycomb-like copper structures obtained by the PO regimes with deposition pulses of: (a) 3 ms; (b) 5 ms; (c) 10 ms; and (d) 20 ms. Pause duration: 10 ms (Reprinted from [41] with permission from Elsevier.)

the hydrogen bubbles in the copper deposit obtained with a deposition 429
pulse of 3 ms are clearly seen from Fig. 4.18a. The analysis of 430
Fig. 4.18b confirmed that more branchy dendrites are formed with a 431
deposition pulse of 5 ms than with 3 ms. Further increase of the 432
deposition pulse led to the increase of a dispersity of the internal 433
structures of the copper deposits, which is observed from Fig. 4.18c, 434
d showing the cross sections of the copper deposits obtained with 435
deposition pulses of 10 and 20 ms. The numbered channels formed 436

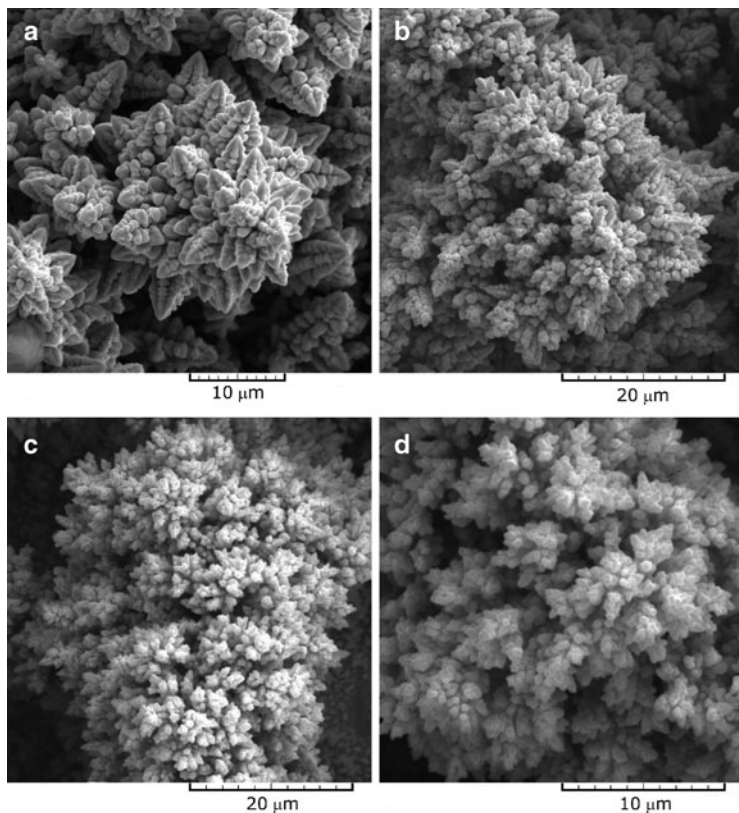


Fig. 4.17 Morphology of electrodeposited copper formed around holes by the PO regimes with deposition pulses of: (a) 3 ms; (b) 5 ms; (c) 10 ms; and (d) 20 ms. Pause duration: 10 ms (Reprinted from [41] with permission from Elsevier.)

437 around relatively small copper particles and degenerate dendrites are
438 easily observed from Fig. 4.18c, d. From Fig. 4.18, it can also be seen
439 that the depth of holes did not change noticeably when deposition
440 pulses of 3, 5, and 10 ms were applied. The depth of the hole obtained
441 with a deposition pulse of 20 ms was larger than those obtained with 3,
442 5, and 10 ms, what can be ascribed to the enhanced dispersity of this
443 deposit. The analysis of holes shown in Fig. 4.18 showed that there

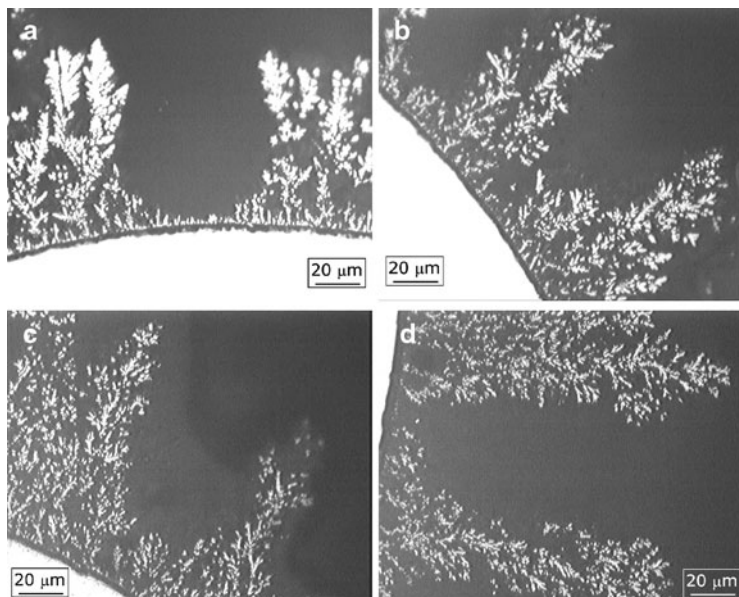


Fig. 4.18 Cross section of the copper deposits obtained with deposition pulses of: (a) 3 ms; (b) 5 ms; (c) 10 ms; and (d) 20 ms. Pause duration: 10 ms (Reprinted from [41] with permission from Elsevier.)

was not any effect of deposition pulse duration on the size of holes. 444
The average diameter of holes obtained with deposition pulses of 3, 5, 445
10, and 20 ms (for pause duration of 10 ms) was estimated to be 446
 $65 \pm 2.0 \mu\text{m}$ [41]. 447

Then, the formation of the honeycomb-like structures by the PO 448
regimes, as well as the change of morphology of the electrodeposited 449
copper from dendrites to degenerate dendrites and cauliflower-like 450
agglomerates of copper grains, can be explained as follows: similar to 451
the constant regimes of electrolysis, in the initial stage of the electro- 452
deposition process, both the nuclei of copper and the “nuclei” of the 453
hydrogen bubbles are formed at the active sites of the electrode 454
surface [18]. The number of the formed hydrogen bubbles is deter- 455
mined by the overpotential amplitude. Since the formed bubbles 456
isolate electrode surface, electrodeposition of copper occurs around 457

458 them forming rings consisted of agglomerates of copper grains.
459 In the growth process, during deposition pulse, due to a concentration
460 of current lines, both copper nucleation and hydrogen evolution
461 primarily occur at these agglomerates of copper grains. Some of the
462 new, freshly formed hydrogen bubbles coalesce with the hydrogen
463 bubbles formed in the initial stage, leading to their growth with
464 electrolysis time.

465 Meanwhile, some of the freshly formed hydrogen bubbles cannot
466 find a path to coalesce with them, and these hydrogen bubbles start to
467 grow independently making an interior of deposit to be porous. Due to
468 a constant value of pause duration of 10 ms, the effect of pause
469 duration was the same for all deposition pulses. During the pause,
470 the dissolution of both copper particles and the formed hydrogen
471 bubbles occur.

472 The prolonging duration of deposition pulse increases both copper
473 deposition and hydrogen evolution rates. This means a greater num-
474 ber of both new hydrogen bubbles and copper “nuclei” is formed
475 with the prolonging deposition pulses. The greater part of these
476 freshly formed bubbles will not find a path to coalesce with the
477 previously formed hydrogen bubbles, because they are surrounded
478 by freshly formed copper grains. Also, they will not be able to
479 develop into large hydrogen bubbles the same reason. Due to impos-
480 sibility for their further growth, these hydrogen bubbles will detach
481 very fast from a growing electrode surface forming a channel struc-
482 ture through the interior of deposit and causing stirring of solution in
483 the near-electrode layer.

484 The analysis of Figs. 4.15–4.18 confirms that the effectiveness of
485 a stirring of solution increased with the increasing duration of depo-
486 sition pulse. Because of the increased effectiveness of a stirring of
487 solution by evolved hydrogen, the change of morphology of the
488 electrodeposited copper from dendrites to degenerate dendrites and
489 cauliflower-like agglomerates was observed.

490 On the basis of the same hole sizes and their unchanged number, as
491 well as of the same depth of holes (Figs. 4.16–4.18), it can be
492 concluded that the critical size of the hydrogen bubbles formed in
493 the initial stage of electrodeposition process to be detached from
494 electrode surface does not depend on the length of deposition pulse.
495 It can be assumed that approximately a same quantity of evolved

hydrogen is used for the formation of these holes. Then, the difference 496
 between this quantity and the overall quantity of evolved hydrogen is 497
 responsible for a stirring of solution and a change of hydrodynamic 498
 conditions in the near-electrode layer. Also, it is clear that the quality 499
 of deposits formed between holes is determined by this difference in 500
 the quantity of evolved hydrogen. 501

4.5.3 Energy Aspects of the Formation of the Honeycomb-Like Structures by the PO Regime 502 503 504

Energy aspects of the formation of these electrodes can be obtained 505
 by the analysis of the specific energy consumption, w , which can be 506
 an important energy parameter in the development of these 507
 electrodes for commercial purposes. For electrodeposition process 508
 in PO regime, the specific energy consumption can be presented by 509
 Eq. (4.1) [41]: 510

$$w = \frac{nF\eta_A}{M(1 - \eta_{l,av}(H_2))}, \quad (4.1)$$

where η_A is the amplitude of overpotential, M is the molar mass of 511
 copper (63,55 g/mol), and the number of Faraday per mole of 512
 consumed ions of copper is $2 \times 26.8 \text{ Ah/mol} = 53.6 \text{ Ah/mol}$. 513
 Using the overpotential amplitude of 1,000 mV, and the values of 514
 $\eta_{l,av}(H_2)$ obtained with deposition pulses of 3 and 10 ms (Table 4.2), 515
 it can be shown that the shortening of deposition pulse from 10 to 516
 3 ms leads to the decrease of the specific energy consumption for 517
 about 15%. Simultaneously, the number, diameter, and depth of holes 518
 remained unchanged. Considering the unchanged number of holes 519
 with the approximate same diameter and depth, it is clear that the use 520
 of shorter deposition pulses showed as a valuable way for energy 521
 saving in a production of this structure type. 522

Aside from energy savings attained by the application of PO regime, 523
 the improvement of mechanical strength of the honeycomb-like 524

t2.1 **Table 4.2** The values of the average current efficiencies of hydrogen evolution, $\eta_{l,av}(H_2)$, in %, the average current efficiencies for copper electrodeposition, $\eta_{l,av}(Cu)$, in %, and the specific energy consumptions obtained for electrodeposition of copper with different pause to pulse ratios

t2.2 t_c (ms)	1	4	7	10	20	Const. regime
t2.3 $\eta_{l,av}(H_2)$ (%)	13.7	20.7	24.4	30.0	32.5	36.0
t2.4 $\eta_{l,av}(Cu)$ (%)	86.3	79.3	75.6	70.0	67.5	64.0
t2.5 w (kWh/kg)	1.075	1.170	1.228	1.326	1.375	1.450

t2.6 Reprinted from [30] with permission from Elsevier
 t_c deposition pulse in ms; t_p pause duration in ms ($t_p = 10$ ms); $j_A = 0.44$ A/cm²

525 structures was noticed in the process of development of these deposits
 526 as possible electrodes. It can be assumed that the increase of mecha-
 527 nical strength is related to the decrease of the quantity of evolved
 528 hydrogen needed for their formation.

529 **4.6 The Regime of Pulsating Current**

530 The regime of pulsating current (PC) consists of a periodic repetition
 531 of square pulses [34, 35], and it is characterized by the amplitude of
 532 the cathodic current density, j_A , the deposition pulse, t_c (on period),
 533 and the pause duration, t_p , in which the system relaxes (off period).
 534 The average current density, j_{av} , is given by Eq. (4.2):

$$j_{av} = \frac{j_A t_c}{t_c + t_p} \quad (4.2)$$

535 or

$$j_{av} = \frac{j_A}{1 + p}, \quad (4.3)$$

536 if

$$p = \frac{t_p}{t_c}, \quad (4.4)$$

537 where p is the pause to pulse ratio.

In the PC regimes, the surface concentration of depositing ions is 538
 only determined by the average current density [34]. Then, the 539
 overpotential amplitude, η_A , can be presented by Eq. (4.5) [43]: 540

$$\eta_A = \frac{b_c}{2.3} \ln \frac{j_{av}(p+1)}{j_0} + \frac{b_c}{2.3} \ln \frac{1}{1 - \frac{j_{av}}{j_L}}, \quad (4.5)$$

where b_c is the cathodic Tafel slope, j_L is the limiting diffusion 541
 current density, and j_0 is the exchange current density. The activation 542
 part of overpotential, η_{act} , is 543

$$\eta_{act} = \frac{b_c}{2.3} \ln \frac{j_{av}}{j_0} (p+1) \quad (4.6)$$

while the diffusion part of overpotential, η_{diff} , is 544

$$\eta_{diff} = \frac{b_c}{2.3} \ln \frac{1}{1 - \frac{j_{av}}{j_L}}. \quad (4.7)$$

Equation (4.5) can be rewritten in the form 545

$$\eta_A = \eta_{const} + \frac{b_c}{2.3} \ln(p+1), \quad (4.8)$$

where η_{const} is the overpotential in the constant regime of electrolysis 546
 defined by Eq. (4.9): 547

$$\eta_{const} = \frac{b_c}{2.3} \ln \frac{j_{av}}{j_0} + \frac{b_c}{2.3} \ln \frac{1}{1 - \frac{j_{av}}{j_L}}, \quad (4.9)$$

if $j_{av} = j$, where j is the current density in the constant regime of 548
 electrolysis. 549

Equation (4.5) is valid in the frequency range 10–100 Hz, where 550
 the frequency is sufficiently high to produce constant concentration 551
 on the surface and sufficiently low that the effect of DC capacity can 552
 be neglected. Hence, in the analyzed frequency range from 10 to 553

554 100 Hz, the surface concentration of depositing ions is constant
 555 and equal to the one in the constant regime at the current density
 556 corresponding to the average current density in the PC regime
 557 [34, 35]. From the point of view of the average current density, it
 558 means that there is not any difference between electrochemical
 559 deposition processes in the constant regimes and PC conditions.
 560 On the other hand, it is very clear from Eq. (4.5) that at the fixed
 561 value of the average current density the amplitude of overpotential
 562 depends on pause to pulse ratio, and it increases with the increasing
 563 pause to pulse ratio.

564 According to Popov and Pavlović [43], the degree of diffusion
 565 control of electrodeposition process, ω , is defined by Eq. (4.10):

$$\omega = \frac{\ln \frac{1}{1 - \frac{j_{av}}{j_L}}}{\ln \frac{j_{av}}{j_0} + \ln(p + 1) + \ln \frac{1}{1 - \frac{j_{av}}{j_L}}}, \quad (4.10)$$

566 and it represents a contribution of diffusion overpotential to total
 567 cathode overpotential. Hence, due to the increase of activation part of
 568 overpotential with the increasing pause to pulse ratio, the degree of
 569 diffusion control will decrease with the increasing pause to pulse ratio,
 570 resulting in the possible change of texture of deposit. It is noteworthy
 571 that it is valid if $j_{av} < j_L$ in the mixed controlled deposition.

572 In the hydrogen codeposition range, the current efficiency for
 573 metal electrodeposition is less than 1, and then the effective average
 574 current density, j_{av}^* , can be presented by Eq. (4.11):

$$j_{av}^* = \frac{\eta_{I,av}(M)j_A}{1 + p}, \quad (4.11)$$

575 where $\eta_{I,av}(M)$ is the average current efficiency for metal
 576 electrodeposition.

577 Since

$$\eta_{I,av}(M) + \eta_{I,av}(H_2) = 1, \quad (4.12)$$

Eq. (4.11) can be rewritten as

578

$$j_{av}^* = \frac{[1 - \eta_{l,av}(H_2)]j_A}{1 + p}, \quad (4.13)$$

and, according to Eqs. (4.3) and (4.11),

579

$$\eta_{l,av}(H_2) = 1 - \frac{j_{av}^*}{j_{av}}. \quad (4.14)$$

In the hydrogen codeposition range, if $j_{av}^* > j_L$, the amplitude of overpotential is related to the hydrogen reduction, increasing with the current density of hydrogen evolution [43]. Equation (4.5) is still valid [43], but it must be modified and adapted to the effect of hydrogen evolution on metal electrochemical deposition process. Then, the modified Eq. (4.5) can be presented by Eq. (4.15):

$$\eta_{A,eff} = \frac{b_c}{2.3} \ln \frac{j_{av}^*(p+1)}{j_0} + \frac{b_c}{2.3} \ln \frac{1}{1 - \frac{j_{av}^*}{j_L^*}}, \quad (4.15)$$

where $\eta_{A,eff}$ represents the effective overpotential amplitude and j_L^* is the effective limiting diffusion current density which depends on the hydrodynamic conditions in the near-electrode layer caused by hydrogen evolution during electrodeposition process. Equation (4.15) is valid if the condition $j_{av}^*/j_L^* < 1$ is fulfilled. The effective average current density, j_{av}^* , can be calculated by the use of Eq. (4.13) if the value of the average current efficiency of hydrogen evolution is known. Meanwhile, the determination of j_{LV}^* when the change of hydrodynamic conditions in the near-electrode layer is caused by hydrogen evolution is not possible. For that reason, the analysis of morphologies of electrodeposited copper obtained in the hydrogen codeposition range showed an excellent tool for the estimation of the change of effectiveness of solution stirring by evolved hydrogen.

It is very clear from the above consideration that the quantities of evolved hydrogen and hence the morphologies of electrodeposited metal will depend strongly on the applied parameters of PC regimes, such as the amplitude of the current density, deposition pulse, and pause duration.

603

604 **4.6.1 Formation of the Honeycomb-Like** 605 **Structures by the PC Regime**

606 In PC regimes, the intensification of hydrogen evolution reaction can
607 be achieved by:

- 608 1. The increase of the current density amplitude and keeping
609 durations of both the deposition pulse and pause constant
- 610 2. The prolonging of a deposition pulse duration and keeping both
611 the current density amplitude and pause duration constant
- 612 3. The shortening of a pause duration and keeping both the current
613 density amplitude and deposition pulse constant

614 Since the second and third ways are closely related, these two
615 ways will be analyzed simultaneously.

616 **4.6.1.1 The Effect of the Current Density Amplitude**

617 Figure 4.19 shows SEM micrographs of copper deposits obtained
618 with the current density amplitudes of 0.20 A/cm^2 (Fig. 4.19a) and of
619 0.44 A/cm^2 (Fig. 4.19b). In both cases, a deposition pulse of 1 ms
620 and a pause duration of 10 ms were applied. In all experiments
621 related to the analysis of the PC regimes, copper electrodeposition
622 was performed from 0.15 M CuSO_4 in 0.50 M H_2SO_4 at room
623 temperature using the vertical stationary cylindrical copper
624 electrodes [30, 44, 45].

625 Very branchy dendrites, small cauliflower-like forms, and shallow
626 holes formed from detached hydrogen bubbles are formed when the
627 amplitude of current density of 0.20 A/cm^2 was applied (Fig. 4.19a).
628 On the other hand, dish-like holes and small cauliflower-like
629 agglomerates of copper grains were formed with a current density
630 amplitude of 0.44 A/cm^2 (Fig. 4.19b). The formation of these
631 morphological forms was accompanied by the quantity of evolved
632 hydrogen which corresponded to the average current efficiency of
633 hydrogen evolution, $\eta_{l,\text{av}}(\text{H}_2)$, of 5.5% with the applied current
634 density amplitude, j_A , of 0.20 A/cm^2 [45], and 13.7% with j_A of
635 0.44 A/cm^2 [30].

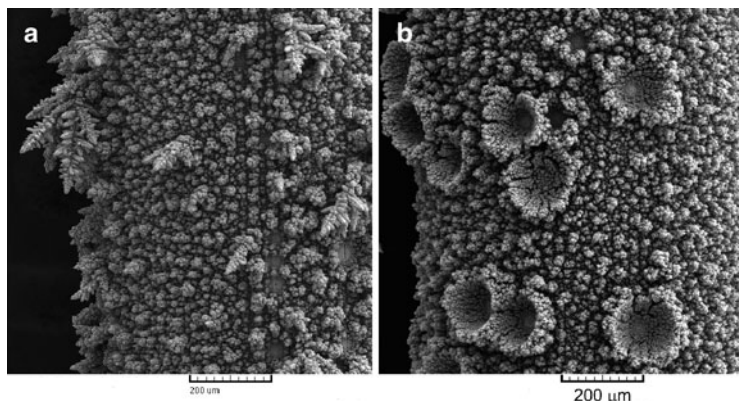


Fig. 4.19 Copper deposits obtained by the regime of pulsating current. The current density amplitude: (a) 0.20 A/cm^2 and (b) 0.44 A/cm^2 . Deposition pulse: 1 ms. Pause duration: 10 ms (Reprinted from [30, 45] with permission from Elsevier.)

4.6.1.2 The Effect of the Length of Deposition Pulse

636

The prolongation of a duration of deposition pulse leads to the formation of honeycomb-like structures with both the current density amplitudes applied [30, 45]. The formation of this structure type is analyzed applying the current density amplitude of 0.44 A/cm^2 , deposition pulses of 1, 4, 7, 10, and 20 ms, and a pause duration of 10 ms [30]. The values of the average current efficiency of hydrogen evolution, $\eta_{l,av}(\text{H}_2)$, obtained for these parameters of PC regimes are given in Table 4.2. Also, the value of $\eta_{l,av}(\text{H}_2)$ obtained for copper electrodeposition at the constant current density of 0.44 A/cm^2 is included in this table.

Using j_A of 0.44 A/cm^2 , the honeycomb-like structures are formed with deposition pulses of 7 ms and longer and the typical honeycomb-like structure obtained with a deposition pulse of 10 ms is shown in Fig. 4.20a. The mixture of dish-like holes and holes constructing the honeycomb-like structure was formed with a deposition pulse of 4 ms (Fig. 4.20b). Finally, as already mentioned, dish-like holes and independently formed agglomerates of copper grains were formed with a deposition pulse of 1 ms (Fig. 4.19b).

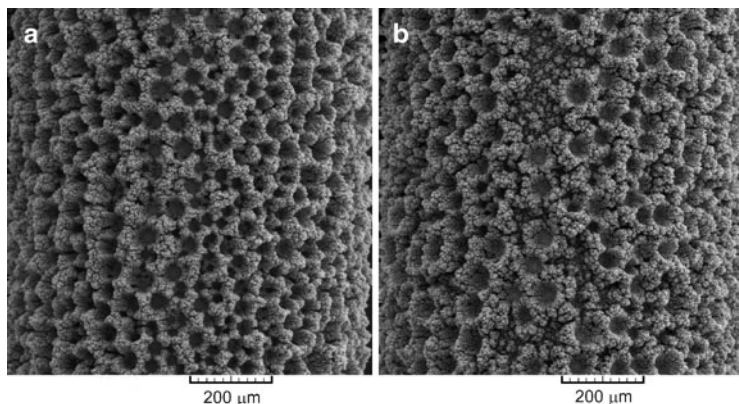


Fig. 4.20 Copper deposits obtained by the PC regimes with a deposition pulse of: (a) 10 ms and (b) 4 ms. Pause duration: 10 ms. The amplitude of current density: 0.44 A/cm^2 (Reprinted from [30] with permission from Elsevier.)

655 The shape, size, and number of holes strongly depended on the
656 length of deposition pulse. The honeycomb-like structure
657 electrodeposited with a deposition pulse of 20 ms was constructed of
658 noncoalesced and coalesced holes (Fig. 4.21a, b, respectively).
659 The decreasing length of deposition pulse led to the suppression of
660 the coalescence process. Noncoalesced holes formed with a deposition
661 pulse of 10 ms were very similar to those obtained with a deposi-
662 tion pulse of 20 ms. Aside from the appearing of slightly larger holes
663 than those formed with the deposition pulse of 10 ms, the decrease of
664 deposition pulse to 7 ms did not have any effect on the shape and the
665 size of holes. The mixture of dish-like holes and the noncoalesced holes
666 constructing the honeycomb-like structure was formed with a deposi-
667 tion pulse of 4 ms [30]. The typical dish-like hole formed with a
668 deposition pulse of 1 ms is shown in Fig. 4.21c.

669 Figure 4.22 shows the dependences of the average diameter of
670 holes and the number of holes per mm^2 surface area of the copper
671 electrode on pause to pulse ratio. In these dependences, the values
672 obtained at the constant current density ($j = 0.44 \text{ A/cm}^2$; $p = 0$) are
673 also included. From Fig. 4.22 can be seen that the size of
674 noncoalesced holes in the honeycomb-like structures did not depend
675 on the length of deposition pulse. As expected, the size of dish-like

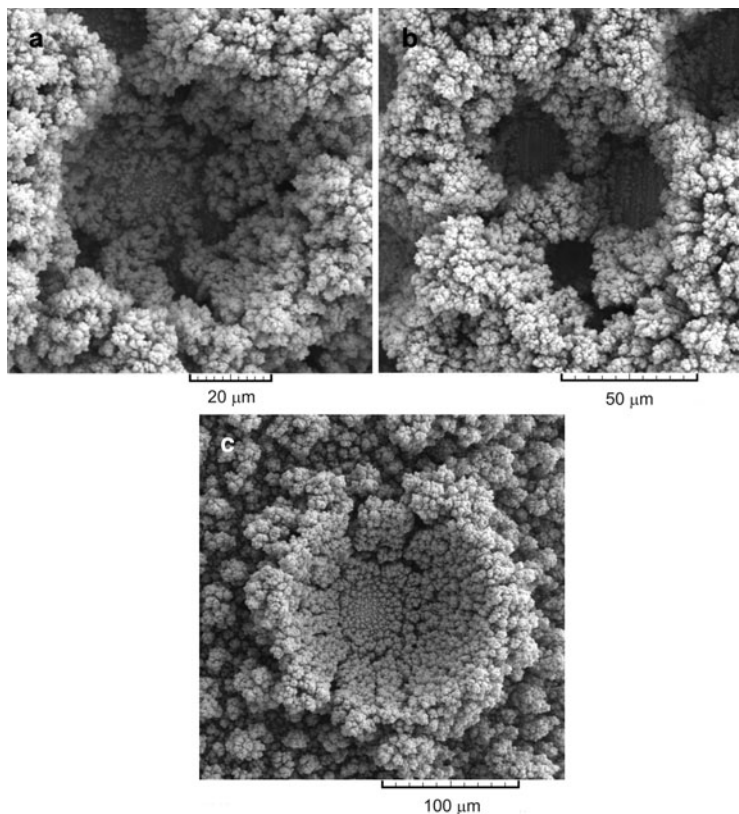


Fig. 4.21 The typical holes formed by the PC regimes with a deposition pulse of: (a) and (b) 20 ms; and (c) 1 ms. Pause duration: 10 ms. The amplitude of current density: 0.44 A/cm^2 (Reprinted from [30] with permission from Elsevier.)

holes was larger than those forming the honeycomb-like structures 676
[19]. On the other hand, the dependence of the number of holes on the 677
pause to pulse ratio shows maximal value for a pause to pulse ratio of 678
1 ($t_c = 10 \text{ ms}$). The increase of number of holes obtained with a 679
pause to pulse ratio of 0.5 ($t_c = 20 \text{ ms}$) in relation to the one formed 680
at the constant current density ($p = 0$) is due to the decreased 681
coalescence of closely formed hydrogen bubbles. The maximum of 682
the dependence obtained for a pause to pulse ratio of 1 ($t_c = 10 \text{ ms}$) 683

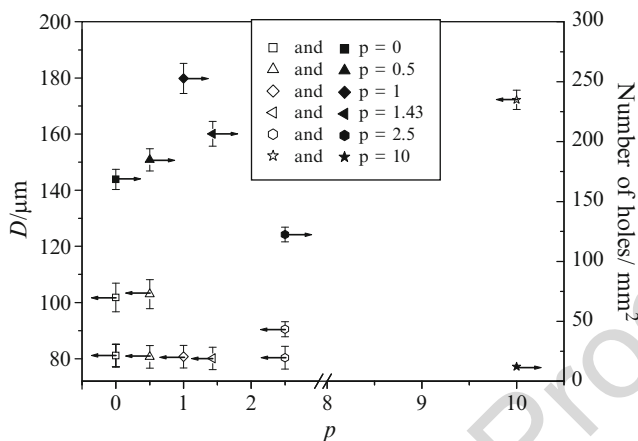


Fig. 4.22 The average diameter, D , and the number of holes per mm^2 surface area of copper electrodes obtained at a constant current density of 0.44 A/cm^2 and for different pause to pulse ratios. Pause duration: 10 ms (Reprinted from [30] with permission from Elsevier.)

684 corresponds to suppressed coalescence of hydrogen bubbles.
 685 The decrease of the number of holes and the appearing of dish-like
 686 holes can be ascribed to the decrease of quantity of evolved hydrogen
 687 and hence to the decrease of the effectiveness of solution stirring by
 688 evolved hydrogen with the increasing pause to pulse ratio.

689 Cauliflower-like agglomerates of copper grains can be classified
 690 into two groups. In the first group are inserted cauliflower-like
 691 agglomerates of copper grains constructing the honeycomb-like
 692 structures. These copper agglomerates are very disperse and
 693 consisted of small agglomerates of copper grains, as shown in
 694 Fig. 4.23a which shows the typical cauliflower-like agglomerates
 695 of copper grains obtained by the square-wave PC with a deposition
 696 pulse of 10 ms. From Fig. 4.23a can be seen that the size of these
 697 small copper grains agglomerates of which large cauliflower-
 698 like agglomerates formed among holes were constructed was about
 699 $4 \mu\text{m}$. Also, the agglomerates of copper grains were surrounded by
 700 irregular channels for which the origin was of evolved hydrogen.
 701 In the second group are inserted cauliflower-like agglomerates

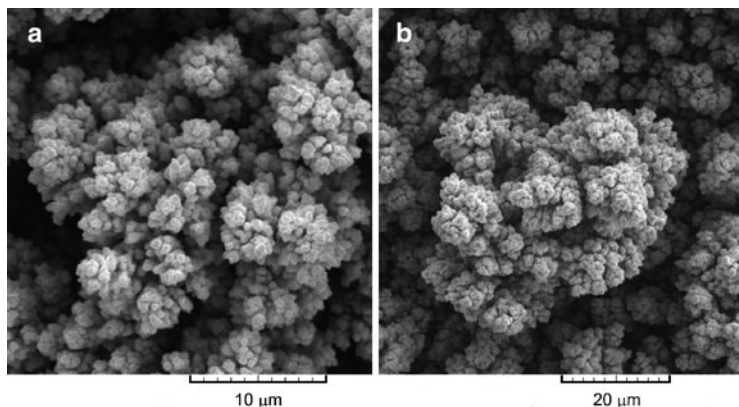


Fig. 4.23 The typical cauliflower-like agglomerates of copper grains formed by the PC regimes with a deposition pulse of: (a) 10 ms and (b) 1 ms. Pause duration: 10 ms (Reprinted from [30] with permission from Elsevier.)

of copper grains formed by the PC regime with a deposition pulse of 702
1 ms. Also, this type of agglomerates can be noticed in the transi- 703
tional structure formed with a deposition pulse of 4 ms. The typical 704
agglomerate of copper grains from this group is given in Fig. 4.23b 705
which shows the one obtained with a deposition pulse of 1 ms. 706
Copper grains agglomerates from this group are formed at the elec- 707
trode surface independently from the formed hydrogen bubbles. They 708
were larger and more compact than those formed among hydrogen 709
bubbles at the constant current density and by the PC regimes with 710
deposition pulses of 7, 10, and 20 ms [30]. 711

Cross section of copper deposits obtained with deposition pulses 712
of 4, 7, 10, and 20 ms is shown in Fig. 4.24. From Fig. 4.24, it can be 713
seen that the interior of these structures was very porous and 714
consisted of disperse particles surrounded by irregular channels for 715
which the origin is of evolved hydrogen [44]. Also, it is necessary to 716
note that dendritic character of these particles decreased with the 717
prolonging duration of deposition pulse. As already mentioned, the 718
porous interior of these deposits is very important for electrocatalytic 719
purposes because the pores facilitate the transport of electroactive 720
species through the interior of the structures, what is very desirable 721

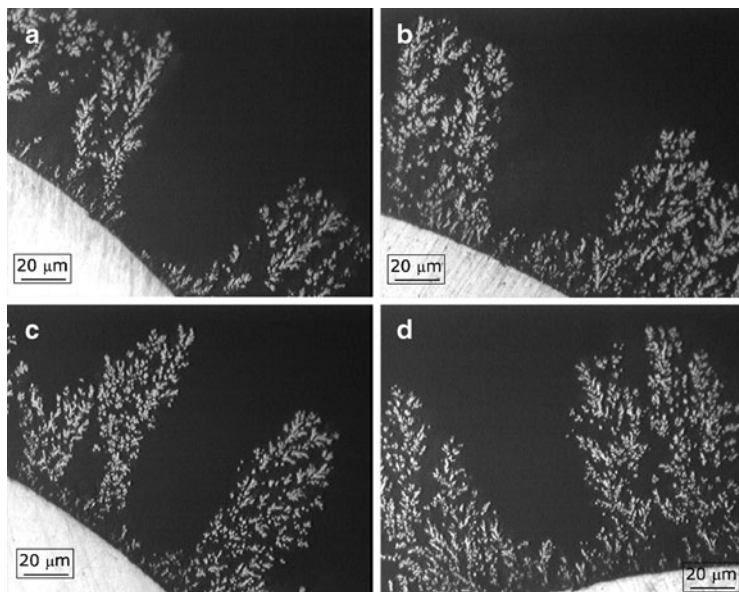


Fig. 4.24 Cross section of the copper deposits obtained by the PC regimes with deposition pulses of: (a) 4 ms; (b) 7 ms; (c) 10 ms; and (d) 20 ms. The current density amplitude: 0.44 A/cm^2 . Pause duration: 10 ms (Reprinted from [44] with permission from Springer.)

722 for the evaluation of electrochemical reactions. For example, copper
723 shows a high activity for nitrate ion reduction [46, 47], as well as for a
724 reaction in which nitrate reduces to ammonia in high yield in aqueous
725 acidic perchlorate and sulfate media [48].

726 **4.6.1.3 Discussion of the Effect of Different Parameters** 727 **of the PC Regimes on Electrodeposition of Copper** 728 **in the Hydrogen Codeposition Range**

729 From the above consideration, the existence of the strong effect of the
730 selected parameters of the square-waves PC on hydrogen evolution
731 reaction and hence morphology of electrodeposited copper is very

clear. The change of morphology of electrodeposited copper from very branchy dendrites and dish-like holes to the honeycomb-like structures can be explained by the analysis of the effectiveness of solution stirring by evolved hydrogen in the following way: the effectiveness of stirring of the solution by hydrogen generated at the cathode surface during electrochemical deposition process increases with intensification of hydrogen evolution reaction. In the one moment, hydrogen evolution will become vigorous enough to cause the decrease of the cathode diffusion layer thickness and the increase of the limiting diffusion current density leading to the change of the hydrodynamic conditions in the near-electrode layer [16]. According to Eqs. (4.5) and (4.10), it means the decrease of the degree of diffusion control of electrodeposition process with intensification of hydrogen evolution reaction. The degree of diffusion control of electrodeposition process will additionally decrease due to the smaller values of the effective average current densities, j_{av}^* , in relation to those obtained in the absence of hydrogen evolution [Eqs. (4.3) and (4.13)]. Then, the overpotential amplitude corresponding to copper electrodeposition will be smaller than the one specified by pulse rectifiers and this value is denoted as effective overpotential amplitude of electrodeposition process and it is presented by Eq. (4.15).

Hence, the effective overpotential amplitude, $\eta_{A,eff}$, decreases with the intensification of hydrogen evolution reaction due to the decrease of the degree of diffusion control of electrodeposition process. So, the validity of the concept of “effective overpotential” can be expanded to include metal electrodeposition in the hydrogen codeposition range by the regime of pulsating current (PC), and then this concept applied for the PC regimes can be denoted as “effective overpotential amplitude” one [44].

Anyway, the decrease of dendritic character of particles and hence the increase of dispersity of particles in the formed honeycomb-like structures (Fig. 4.24), as well as the change of the surface morphology from dendrites (Fig. 4.19a) to agglomerates of grains formed around holes (Fig. 4.23a), clearly confirm the decrease of the degree of the diffusion control of electrodeposition process with the increase of the quantity of evolved hydrogen. The different degree of diffusion

769 control of electrodeposition process is attained by the choice of
770 parameters of the square-waves PC. For example, using the value
771 $j_A = 0.20 \text{ A/cm}^2$, $t_c = 1 \text{ ms}$, and $t_p = 10 \text{ ms}$, as well as $\eta_{\text{L,av}}(\text{H}_2)$
772 $= 5.5\%$, the effective average current density, j_{av}^* , calculated by the
773 use of Eq. (4.13) was very close to the value of the limiting diffusion
774 current density for this system (i.e., for 0.15 M CuSO_4 in 0.50 M
775 H_2SO_4 ; $j_L \approx 16.0 \text{ mA/cm}^2$) [16]. Hence, with these parameters of the
776 PC regimes, electrodeposition process was controlled by the diffu-
777 sion of ions to the electrode surface, what is confirmed by the
778 formation of very branchy dendrites and small cauliflower-like
779 agglomerates of copper grains (Fig. 4.19a). Anyway, the nonuniform-
780 ity of the electrode surface clearly pointed out that the diffusion
781 layer of the macroelectrode was not disturbed by evolved hydrogen
782 during this electrodeposition process.

783 On the other hand, the increase of the effectiveness of solution
784 stirring, the decrease of the cathode diffusion layer thickness, and the
785 increase of the limiting diffusion current density occur with the
786 intensification of hydrogen evolution reaction leading to the forma-
787 tion of the honeycomb-like structures. The uniform distribution of
788 morphological forms, i.e., holes and copper grains agglomerates,
789 means the existence of the same hydrodynamic conditions over the
790 whole electrode surface [19]. The size of grains in cauliflower-like
791 agglomerates approached to nanosized dimensions with the intensifi-
792 cation of hydrogen evolution reaction, as shown in Fig. 4.25 for
793 cauliflower-like ones obtained with $t_c = 20 \text{ ms}$. From Fig. 4.25, it
794 can be clearly seen that the size of grains in these agglomerates is
795 between 100 and 300 nm . Also, the porosity of the honeycomb-like
796 structures was additionally increased by numerous nanopores
797 situated between copper grains, as observed from Fig. 4.25.
798 The increased effectiveness of the solution stirring by evolved hydro-
799 gen with the intensification of hydrogen evolution can also be noticed
800 by the analysis of the internal structures of the honeycomb-like
801 deposits shown in Fig. 4.24. The decrease of dendritic character of
802 particles and hence the increase of dispersity of deposits is just a
803 consequence of the increased effectiveness of the solution stirring by
804 evolved hydrogen with the intensification of hydrogen evolution
805 reaction caused by the prolongation of deposition pulse duration.

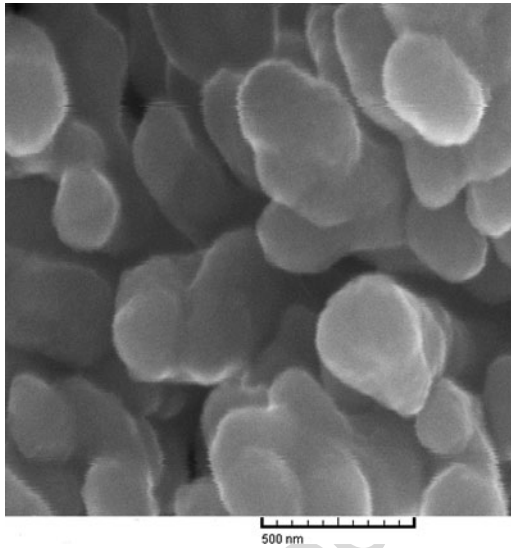


Fig. 4.25 Copper grains agglomerates obtained by the PC regime with a current density amplitude of 0.44 A/cm^2 , a deposition pulse of 20 ms, and a pause duration of 10 ms (Reprinted from [44] with permission from Springer.)

4.6.2 Optimization of the Formation of the Honeycomb-Like Structure by the PC Regime 806
807
808

For the galvanostatic mode of operation, the specific energy consumption, w , defined as the energy spent in the process per unit mass of deposited copper, may be expressed according to [49] by Eq. (4.16): 809
810
811

$$w = \frac{nF \int_0^t U(t) dt}{M \int_0^t \eta_{l,Cu}(t) dt} \tag{4.16}$$

or by Eq. (4.17) as 812

$$w = \frac{nFU_{av}}{M\eta_{l,av}(Cu)}, \tag{4.17}$$

813 where

$$U_{av} = (1/t) \int_0^t U(t)dt \quad (4.18)$$

814 and

$$\eta_{l,av}(\text{Cu}) = (1/t) \int_0^t \eta_{l,\text{Cu}}(t)dt. \quad (4.19)$$

815 According to Eq. (4.17) the specific energy consumption depends
 816 on the average cell voltage, U_{av} , and the average current efficiency
 817 for copper electrodeposition reaction, $\eta_{l,av}(\text{Cu})$. The values of the
 818 average current efficiencies for copper electrodeposition, $\eta_{l,av}(\text{Cu})$,
 819 were calculated using data from Table 4.2 as $\eta_{l,av}(\text{Cu}) = 100 - \eta_{l,av}(\text{H}_2)$,
 820 and the obtained values are added to Table 4.2. The values
 821 of the average cell voltages, U_{av} , can be calculated by Eq. (4.18)
 822 using the experimentally determined dependences of the cell
 823 voltages, U , on time t [30]. The tendency of the decrease of the
 824 average cell voltages was observed with the shortening deposition
 825 pulse and these values were smaller than the average cell voltage
 826 obtained at constant current density of 0.44 A/cm^2 [30].

827 In square-wave PC regimes, the average current density and the
 828 average cell voltage depend on pause to pulse ratio in a similar way.
 829 Hence, the average cell voltage, U_{av} , in a function of p can be given
 830 by Eq. (4.20) [34, 35]:

$$U_{av} = \frac{U_A}{p + 1}, \quad (4.20)$$

831 where U_A is the amplitude cell voltage, if there is no rest cell voltage
 832 during pause duration. In this study, the constant current density used
 833 in DC regime ($j = 0.44 \text{ A/cm}^2$) was equal to the amplitude of current
 834 density in the PC regimes. Consequently, the cell voltage in
 835 the DC regime was used as the amplitude value in the PC regimes
 836 [30]. Then, the amplitude cell voltage, U_A , can be calculated as
 837 $U_A = (1/t) \int_0^t U(t)dt$, where U is the cell voltage in a time t for a
 838 constant regime of electrolysis, and the value of 1.1 V was obtained.

Anyway, the difference between the experimentally determined dependences and calculated in this way was observed and it can be ascribed to the existence of rest voltage during pause. Due to this rest voltage making the cell voltage during pause to be higher than zero, the amplitude cell voltage cannot be calculated by the experimentally measured average cell voltage using Eq. (4.20).

For that reason, assuming that the value of the peak voltage during deposition pulse will not be higher than the cell voltage in constant current mode, the average cell voltage obtained at the constant current density ($p = 0$) was used for the calculation of the specific energy consumption. Then, using the values of the average current efficiencies for copper electrodeposition reaction from Table 4.2 and the average cell voltage of 1.1 V obtained at the constant current density of 0.44 A/cm², the values of the specific energy consumption are calculated and added to Table 4.2.

From Table 4.2, it can be seen that the shortening of deposition pulse led to the decrease of the specific energy consumption, and the obtained values were smaller than the one obtained in the constant mode. On the other hand, the increasing deposition pulse duration favored the formation of the honeycomb-like electrodes. This enabled the optimization process of the formation of the honeycomb-like copper electrodes by the choice of the appropriate parameters of square-waves PC. As already mentioned, the honeycomb-like structures were formed with the pause to pulse ratio smaller than 1.43 (or with the deposition pulse of 7 ms and larger, and a pause duration of 10 ms). It is clear that energy saving of 15.3% was attained by the production of the honeycomb-like electrode by the square-wave PC with a deposition pulse of 7 ms ($p = 1.43$) in comparison to the one obtained at the constant current density. Simultaneously, the increase of the specific surface area of the honeycomb-like electrodes, manifested by the increase of the number of holes due to the suppressed coalescence of closely formed hydrogen bubbles, was observed by the application of these PC regimes (Fig. 4.22).

Anyway, the use of the appropriate square-waves PC enabled energy saving in the production of the honeycomb-like electrodes. In this moment, the largest problem for the commercial manufacturing of open porous structures by the PC regimes is high cost of a pulse rectifier which is much greater than a DC unit [50].

877 It is a highly regulated and sophisticated design that costs more to
878 manufacture. At the first sight, energy savings attained by the appli-
879 cation of the PC regimes and high cost of production of pulse rectifier
880 are in contradiction, but further development of the electronic indus-
881 try will probably decrease the cost of these rectifiers and will enable
882 their larger application in electrochemical technologies.

883 For the technological application of open porous structures as
884 possible electrodes in electrochemical devices, the deposit structural
885 stability of these deposits determined by their adhesion with electrode
886 surface is also very important. It is a well-known fact that the adhesion
887 of deposits is closely associated with the quantity of hydrogen by
888 which metal deposits are formed [51]. At high current densities,
889 dendritic deposits are initiated on the cathode with simultaneous
890 evolution of hydrogen gas. At higher current density, the deposit
891 structure becomes more open, nonuniform, and finer, due to the
892 increased nucleation rate and hydrogen evolution on the cathode
893 [51]. Also, similar effects on copper deposit morphology are observed
894 in potentiostatic regime of electrolysis. Increasing overpotential
895 intensifies the hydrogen evolution reaction causing the change of
896 morphology of electrodeposited copper from dendrite to the honey-
897 comb-like structure constructed of holes formed by the attached
898 hydrogen bubbles with cauliflower-like copper grains agglomerates
899 among them [16]. The mechanical strength of the copper deposits
900 decreases with the increasing current density and hence with the
901 increasing quantity of evolved hydrogen what is proven by the
902 measurement of adhesion of copper deposits by the peel
903 strength test [51]. Hence, it can be concluded by this analysis that
904 the mechanical strength of the honeycomb-like copper structures
905 was improved by the application of PC regimes due to the decrease
906 of the average current efficiency of hydrogen evolution by which they
907 are formed.

908 Hence, the following conveniences in the production of open
909 porous structures, denoted as 3-D foam or the honeycomb-like one,
910 are attained since the appropriate square-waves PC parameters
911 were selected: (a) energy saving, (b) the increase of the specific
912 surface area of the electrodes, and (c) probably the improvement of
913 the deposit structural stability due to the decrease of the quantity of
914 evolved hydrogen needed for their formation. Also, it is clear that the

benefits attained by the application of the pulsating overpotential (PO) regime can be successfully transferred to technological attractive pulsating current (PC) regime.

4.7 The Regime of Reversing Current

The regime of reversing current (RC) is characterized by the cathodic current density, j_c , and the anodic current density, j_a , as well as by the duration of flow of the current in the cathodic and the anodic directions, t_c and t_a , respectively [34, 35]. The average current density, j_{av} , is given by Eq. (4.21):

$$j_{av} = \frac{j_c t_c - j_a t_a}{t_c + t_a} \quad (4.21)$$

or

$$j_{av} = \frac{j_c - j_a r}{1 + r}, \quad (4.22)$$

if

$$r = \frac{t_a}{t_c}. \quad (4.23)$$

For the RC regime in the millisecond range, the surface concentration of the depositing ions is determined by the average current density [34, 35], and the overpotential amplitude, η_A , can be presented by Eq. (4.24):

$$\eta_A = \frac{b_c}{2.3} \ln \frac{j_{av}(r+1) + j_a r}{j_0} + \frac{b_c}{2.3} \ln \frac{1}{1 - \frac{j_{av}}{j_L}}. \quad (4.24)$$

Equation (4.24) is valid in the frequency range 10–100 Hz, where the frequency is sufficiently high to produce constant concentration

932 on the surface and sufficiently low that the effect of DC capacity can
 933 be neglected. It is noteworthy that it is valid if $j_{av} < j_L$ in the mixed
 934 controlled deposition.

935 With the applied cathodic current density pulses larger than the
 936 limiting diffusion current density, parallel to copper electrodeposi-
 937 tion hydrogen evolution reaction occurs [52]. On the other hand,
 938 there was not any gas evolution during anodic pulses indicating
 939 that the overall gas evolution corresponds to hydrogen evolution.
 940 Then, Eq. (4.22) can be modified by Eq. (4.25):

$$j_{av}^* = \frac{\eta_{l,c}(\text{Cu})j_c - j_a r}{1 + r}, \quad (4.25)$$

941 where j_{av}^* is the effective average current density and $\eta_{l,c}(\text{Cu})$ is the
 942 current efficiency for copper electrodeposition during cathodic
 943 pulses. Since $\eta_{l,c}(\text{Cu}) + \eta_{l,c}(\text{H}_2) = 1$, Eq. (4.25) can be presented as

$$j_{av}^* = \frac{[1 - \eta_{l,c}(\text{H}_2)]j_c - j_a r}{1 + r}, \quad (4.26)$$

944 where $\eta_{l,c}(\text{H}_2)$ is the current efficiency for hydrogen evolution reac-
 945 tion during cathodic pulses. For $j_{av}^* > j_L$, the overpotential ampli-
 946 tude is related to the hydrogen reduction, increasing with the current
 947 density of hydrogen evolution [43], and the modified Eq. (4.24) can
 948 be presented as

$$\eta_{A,\text{eff}} = \frac{b_c}{2.3} \ln \frac{j_{av}^* (r + 1) + j_a r}{j_0} + \frac{b_c}{2.3} \ln \frac{1}{1 - \frac{j_{av}^*}{j_L}}, \quad (4.27)$$

949 where $\eta_{A,\text{eff}}$ is the effective overpotential amplitude and j_L^* is the
 950 effective limiting diffusion current density. Naturally, $j_{av}^* < j_L^*$.

951 The regime of pulsating current (PC) represents the special case of
 952 the reversing current (RC) regime ($j_a = 0 \text{ mA/cm}^2$). For that reason,
 953 copper electrodeposition processes in the hydrogen codeposition
 954 range by the RC regimes with the different anodic current density
 955 values are compared with those obtained by the PC regime.

Table 4.3 The values of the average current efficiencies of hydrogen evolution, $\eta_{l,av}(H_2)$, in %, obtained for electrodeposition of copper with different anodic current densities t3.1

j_a (mA/cm ²)	0	40	240	440	640	t3.2
$\eta_{l,av}(H_2)$ (%)	30.7	28.9	25.6	21.7	19.3	t3.3

Reprinted from [52] with permission from Elsevier
 j_a the anodic current density in mA/cm²

4.7.1 The Effect of the Anodic Current Density on the Formation of the Honeycomb-Like Electrodes 956
 957
 958

In all PC and RC experiments, the cathodic current density (or the current density amplitude in the PC regime) of 0.44 A/cm², the cathodic time (or deposition pulse) of 10 ms, and the anodic time (or pause duration) of 5 ms were applied, while the analyzed anodic current densities were 0.040, 0.24, 0.44, and 0.64 A/cm². Copper was electrodeposited from 0.15 M CuSO₄ in 0.50 M H₂SO₄ at the room temperature using cylindrical copper working electrodes. The values of the average current efficiencies of hydrogen evolution calculated as $\eta_{l,av}(H_2) = (1/t) \int_0^t \eta_l(H_2) dt$ for the analyzed PC and RC regimes are presented in Table 4.3. 959
 960
 961
 962
 963
 964
 965
 966
 967
 968

Morphologies of copper deposits obtained by the PC regime and RC regimes with different anodic current densities are shown in Fig. 4.26. Holes formed of detached hydrogen bubbles and agglomerates of copper grains or dendrites were obtained with all analyzed PC and RC regimes. From Fig. 4.26, it can be seen that the honeycomb-like structures are formed by the PC regime and by the RC regimes with the anodic current densities up to 440 mA/cm². Holes obtained by a coalescence of closely formed hydrogen bubbles are noticed by the analysis of the honeycomb-like structures formed by the PC regime (Fig. 4.27a) and the RC regime with j_a of 40 mA/cm². In the range of the examined anodic current densities from 0 (the PC regime) to 440 mA/cm², holes constructing the honeycomb-like structures (so-called “noncoalesced” one) were similar to each other, and the typical hole of this type obtained with 969
 970
 971
 972
 973
 974
 975
 976
 977
 978
 979
 980
 981
 982

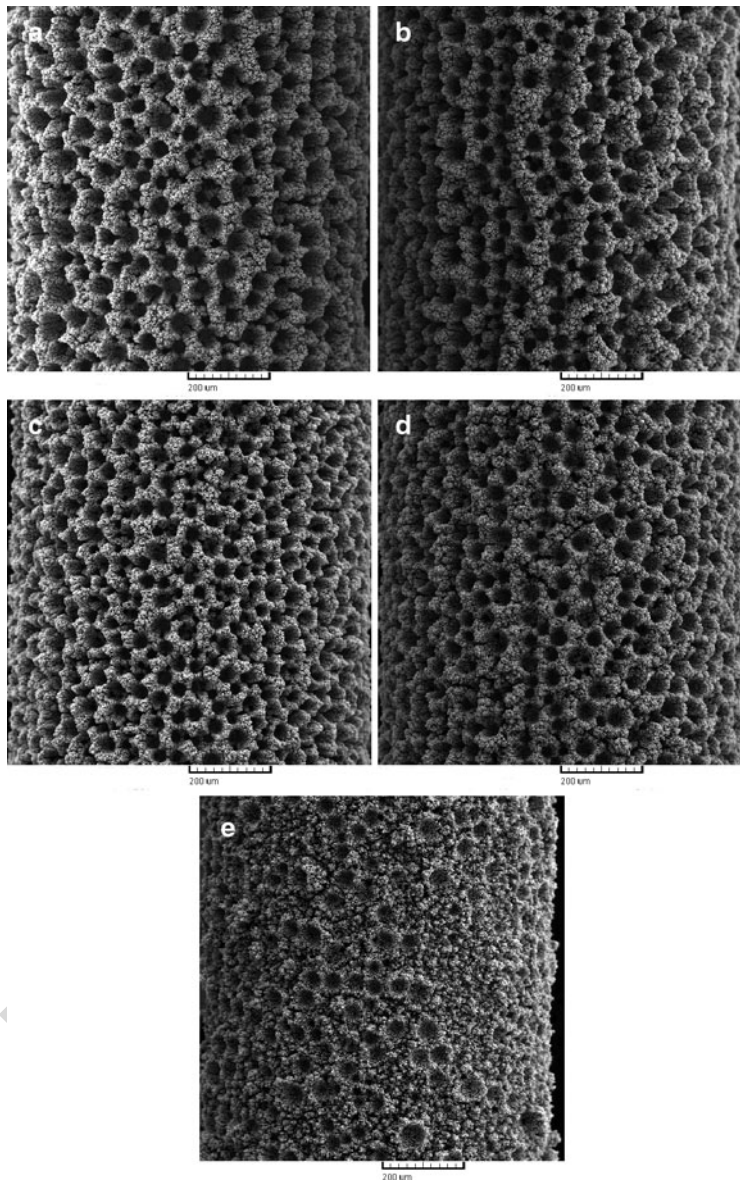


Fig. 4.26 Copper deposits obtained by: (a) the PC regime and by the RC regimes with the anodic current density j_a of: (b) 40; (c) 240; (d) 440 and (e) 640 mA/cm². The cathodic current density j_c : 440 mA/cm², the cathodic pulse t_c : 10 ms, and the anodic pulse, t_a : 5 ms (Reprinted from [52] with permission from Elsevier.)

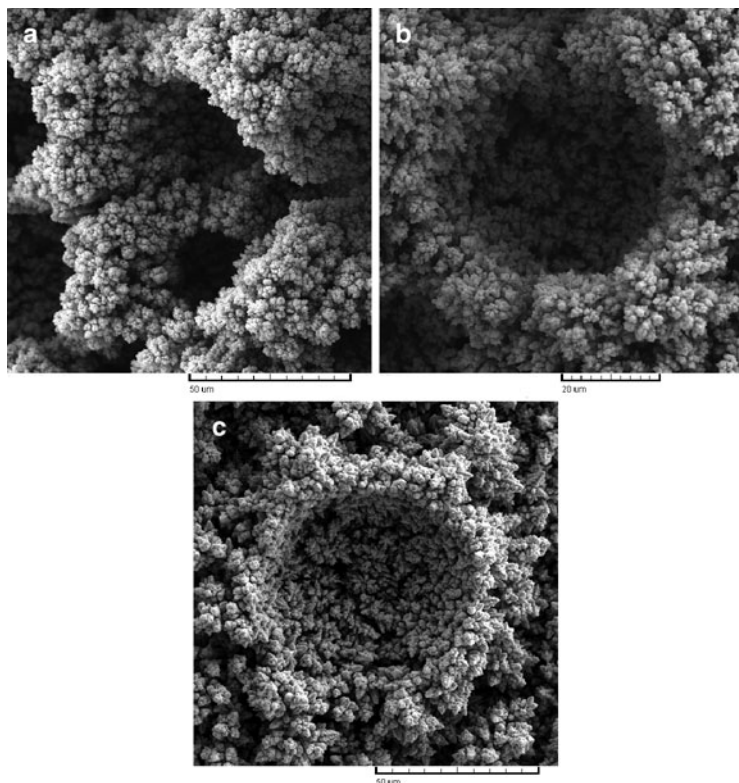


Fig. 4.27 The types of holes formed of detached hydrogen bubbles by different PC and RC regimes: (a) coalesced hole obtained by the PC regime; (b) noncoalesced hole obtained by the RC regime with $j_a = 440 \text{ mA/cm}^2$ and (c) dish-like hole obtained by the RC regime with $j_a = 640 \text{ mA/cm}^2$. The cathodic current density j_c : 440 mA/cm^2 , the cathodic pulse t_c : 10 ms, and the anodic pulse, t_a : 5 ms (Reprinted from [52] with permission from Elsevier.)

j_a of 440 mA/cm^2 is shown in Fig. 4.27b. Finally, dish-like holes were 983
dominant type of holes obtained with j_a of 640 mA/cm^2 (Fig. 4.27c). 984

Figure 4.28 shows the dependences of the average diameter and the 985
number of holes formed at electrode surface in a function of the anodic 986
current density. The average size and number of holes obtained for 987
the PC regime ($j_a = 0 \text{ mA/cm}^2$) are also included in this figure. 988

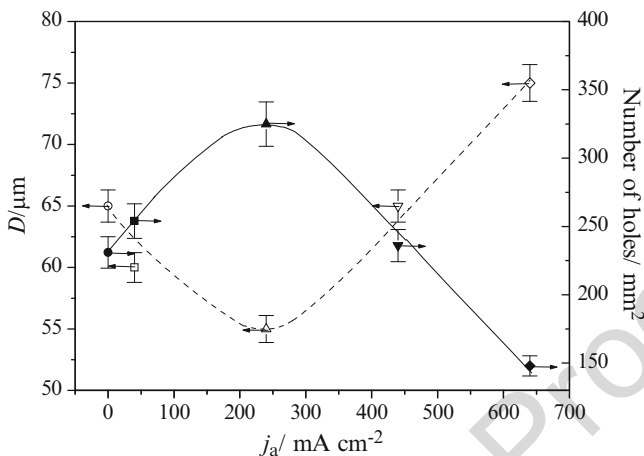


Fig. 4.28 The dependences of the average diameter, D , and the number of holes per mm^2 surface area of copper electrodes on the anodic current density value. The cathodic current density j_c : 440 mA/cm^2 , the cathodic pulse t_c : 10 ms , and the anodic pulse t_a : 5 ms (Reprinted from [52] with permission from Elsevier.)

989 The average diameter of holes obtained by coalescence of closely
 990 formed hydrogen bubbles was larger than the average diameter of
 991 “noncoalesced” holes, and the size of these holes is not presented in
 992 Fig. 4.28. From Fig. 4.28, it can be seen that the dependence of the
 993 average diameter of holes on the anodic current density is of a para-
 994 bolic shape with a minimum at $j_a = 240 \text{ mA/cm}^2$. On the other hand,
 995 the dependence of the number of the holes per mm^2 surface area of
 996 the electrode on the anodic current density value had the shape of
 997 reverse parabola with the maximal number of holes formed with
 998 $j_a = 240 \text{ mA/cm}^2$. Due to the existence of holes formed by coales-
 999 cence process, the overall number of holes formed by both the PC
 1000 regime and the RC regime with $j_a = 40 \text{ mA/cm}^2$ was smaller than the
 1001 one formed by the RC regime with $j_a = 240 \text{ mA/cm}^2$. The decrease of
 1002 the number of holes with the anodic current density larger than j_a
 1003 $= 240 \text{ mA/cm}^2$ can be ascribed to the strong effect of the anodic
 1004 current densities on both the hydrogen evolution reaction and copper
 1005 electrodeposition rate.

Morphologies of copper deposits formed around holes are shown in Fig. 4.29. The change of morphology of the electrodeposited copper from cauliflower-like agglomerates of copper grains to dendrites was observed with the increasing anodic current density values. Cauliflower-like agglomerates of copper grains obtained by the regimes of PC (Fig. 4.29a) and RC with $j_a = 40 \text{ mA/cm}^2$ (Fig. 4.29b) are very disperse, and the presence of deep irregular channels of detached hydrogen bubbles [19] formed around small copper grains agglomerates was easily noticed. From Fig. 4.29a, b, it can be clearly seen that these cauliflower-like agglomerates of copper grains are very similar to each other, what is understandable due to the absence or the small value of the anodic component of the current density in comparison with the cathodic current density. With the increasing anodic current density, deep irregular channels around small copper agglomerates were lost making the honeycomb-like structures obtained with $j_a = 240 \text{ mA/cm}^2$ (Fig. 4.26c) and $j_a = 440 \text{ mA/cm}^2$ (Fig. 4.26d) more compact than those obtained in the PC regime (Fig. 4.26a) and the RC regime with $j_a = 40 \text{ mA/cm}^2$ (Fig. 4.26b). Also, holes approached each other (or the wall width decreased) with the increase of the anodic current density (Fig. 4.29a–c). The increase of the anodic current density led to the formation of dendrites on the top of agglomerates of copper grains (Fig. 4.29d). Finally, very branchy dendrites were formed with $j_a = 640 \text{ mA/cm}^2$ (Fig. 4.29e).

The increase of the compactness of the honeycomb-like structures can be explained by the strong effect of the anodic current density on both the hydrogen evolution reaction and copper electrodeposition rate as follows: in the growth process, due to the current density distribution effect, during cathodic pulses both the copper nuclei and the hydrogen bubbles are primarily formed at the top of agglomerates of grains formed around initially formed hydrogen bubbles. During anodic pulses, due to the same effect, the anodic current density (or the anodic current lines) will be concentrated at the top of these freshly formed copper nuclei causing their dissolution. The dissolution process of copper nuclei facilitates to freshly formed hydrogen bubbles to find path to coalesce with initially formed hydrogen bubbles leading to their growth with electrolysis time. With the increasing anodic current density, the dissolution of copper

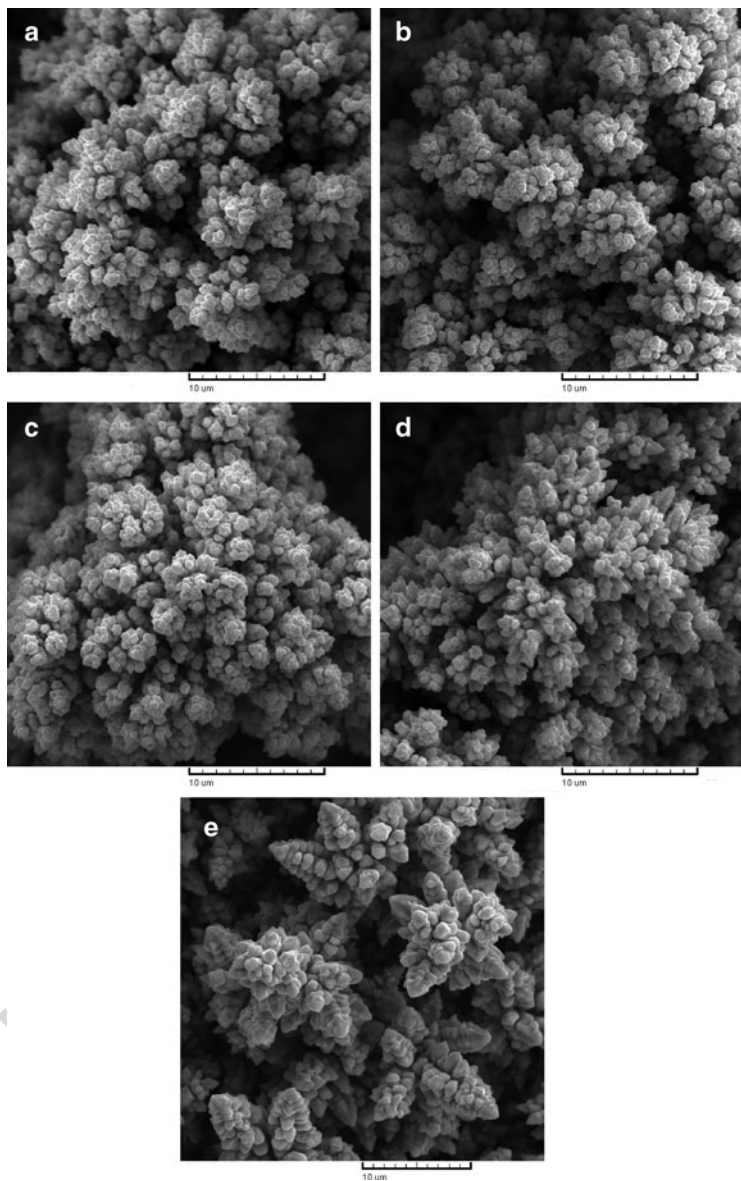


Fig. 4.29 Morphology of electrodeposited copper formed around holes by: (a) the PC regime and by the RC regimes with the anodic current density j_a of: (b) 40; (c) 240; (d) 440 and (e) 640 mA/cm². The cathodic current density j_c : 440 mA/cm², the cathodic pulse t_c : 10 ms, and the anodic pulse t_a : 5 ms (Reprinted from [52] with permission from Elsevier.)

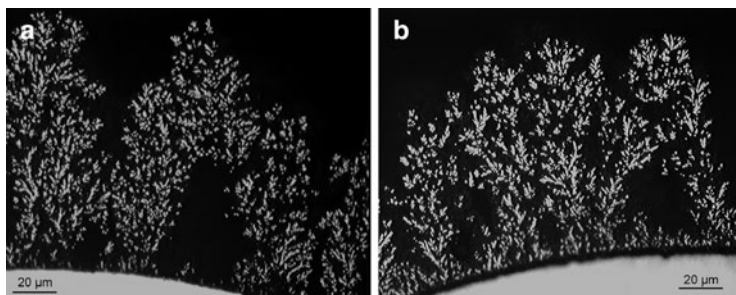


Fig. 4.30 Cross section of the honeycomb-like deposits obtained with: (a) $j_a = 40 \text{ mA/cm}^2$ and (b) $j_a = 440 \text{ mA/cm}^2$. The cathodic current density j_c : 440 mA/cm^2 , the cathodic pulse t_c : 10 ms, and the anodic pulse t_a : 5 ms (Reprinted from [52] with permission from Elsevier.)

nuclei increases, and the number of freshly formed hydrogen bubbles 1044
which will coalesce with the initially formed hydrogen bubbles is 1045
increased. Simultaneously, the number of hydrogen bubbles which 1046
will remain trapped among freshly formed copper nuclei and 1047
constructing channel structure through the interior of the deposit is 1048
decreased. It means that these simultaneous processes will lead to a 1049
reduction of irregular channels formed around small copper grains 1050
agglomerates, and hence, up to the increase of the compactness of the 1051
honeycomb-like structures. 1052

Anyway, the ratio of hydrogen creating channel structure to the 1053
overall quantity of evolved hydrogen decreases with the increasing 1054
anodic current density values. Also, due to the increasing dissolution 1055
effect, the size of grains constructing agglomerates decreased with 1056
the increase of the anodic current density. 1057

The complete insight into the strong effect of the anodic current 1058
density on the macromorphology of copper deposits is obtained by the 1059
analysis of their internal structures. Figure 4.30 shows cross sections 1060
of the honeycomb-like deposits obtained with $j_a = 40 \text{ mA/cm}^2$ 1061
(Fig. 4.30a) and $j_a = 440 \text{ mA/cm}^2$ (Fig. 4.30b). At the first sight, a 1062
clear difference in the internal structures of these copper deposits can 1063
be seen by the analysis of Fig. 4.30. The interior of copper deposit 1064
obtained with $j_a = 40 \text{ mA/cm}^2$ was constructed from fine particles 1065
(Fig. 4.30a), while a well-defined dendritic structure can be noticed in 1066

1067 the copper deposit obtained with $j_a = 440 \text{ mA/cm}^2$ (Fig. 4.30b). The
1068 second strong effect of the increasing anodic current density on the
1069 internal structure of the copper deposits was related to the shape of
1070 cavities formed in the interior of deposits. The absence of the deposit
1071 at the bottom of the cavity and its regular shape close to the electrode
1072 surface following the shape of hydrogen bubbles clearly indicate that
1073 the origin of the cavity in the deposit obtained with $j_a = 40 \text{ mA/cm}^2$ is
1074 of hydrogen bubbles formed at the electrode surface in the initial stage
1075 of electrodeposition. The formed hydrogen bubbles isolate the elec-
1076 trode surface preventing the growth of deposit at the position of their
1077 formation. In the growth process, due to the current density distribu-
1078 tion effect, they remained included in the interior of deposit making
1079 this deposit type to be very porous. This type of cavity is not found in
1080 the copper deposits obtained with the larger anodic current densities
1081 indicating that the increase of the number of holes formed of detached
1082 hydrogen bubbles (Fig. 4.28) can be not only ascribed to suppressed
1083 coalescence of closely formed hydrogen bubbles but also to the
1084 improved current density distribution at the growing electrode sur-
1085 face. The second type of the cavity had irregular shape (Fig. 4.30b)
1086 and this cavity type is formed by the overlap of closely formed
1087 branchy dendrites. From Fig. 4.30b, it can be seen that before the
1088 overlap of dendrites, copper electrodeposition occurred over the whole
1089 electrode surface. The improvement of the current density distribution
1090 effect was observed with the increasing anodic current density.

1091 The formation of dendrites instead of fine particles can be
1092 explained by the decrease of the quantity of the hydrogen generated
1093 during copper electrochemical deposition processes with the increase
1094 of the anodic current density as follows: due to the decrease of the
1095 quantity of evolved hydrogen which leads to a stirring of solution in
1096 the near-electrode layer, the thickness of the diffusion layer increases
1097 and the limiting diffusion current density decreases causing the
1098 increase of the degree of diffusion control of the electrodeposition
1099 process. From the point of view of mechanism of the electrodeposi-
1100 tion processes in the hydrogen codeposition range, it means that the
1101 effective overpotential amplitude, $\eta_{A,\text{eff}}$ [Eq. (4.27)] will increase
1102 with the increasing anodic current density. The change of morpho-
1103 logy of the electrodeposited copper from very disperse agglomerates
1104 of copper grains to branchy dendrites (Fig. 4.29) clearly points out

the increase of the degree of diffusion control of the electrodeposition process with the increasing anodic current density. 1105 1106

4.7.1.1 Analysis of the Applied Regimes of RC on Both the Specific Surface Area and the Structural Stability 1107 1108

On the basis of the maximal number of holes and the minimal wall width (or the distance among holes), it is clear that the largest specific surface area of the honeycomb-like electrode is obtained by the RC regime with $j_a = 240 \text{ mA/cm}^2$. 1109 1110 1111 1112

As already mentioned, the average current efficiency of hydrogen evolution decreased with the increasing anodic current density. In the range of the anodic current densities from 0 (the PC regime) to 440 mA/cm^2 which enabled the formation of the honeycomb-like electrodes, the decrease of $\eta_{I,av}(\text{H}_2)$ of 29.3% was reached. The honeycomb-like electrode with the maximal specific surface area (the RC regime with $j_a = 240 \text{ mA/cm}^2$) was formed with 16.6% smaller the average current efficiency of hydrogen evolution than the one obtained by the PC regime. The change of $\eta_{I,av}(\text{H}_2)$ was increased when the comparison between the average current efficiencies of hydrogen evolution obtained for the honeycomb-like structures formed in the constant galvanostatic regime at the current density which corresponded to the cathodic current density of 440 mA/cm^2 and the RC regime with $j_a = 240 \text{ mA/cm}^2$ was made. In the constant regime of electrolysis, at $j = 440 \text{ mA/cm}^2$, $\eta_{I,av}(\text{H}_2) = 36.0\%$ [30], the decrease of $\eta_{I,av}(\text{H}_2)$ of 28.9% was obtained. It is well known fact that the structural stability of a deposit is closely associated with the quantity of hydrogen evolved at the electrode surface during the electrodeposition process [51]. The smaller the quantity of evolved hydrogen, the better structural stability of a deposit is obtained. The decrease of a quantity of evolved hydrogen spent for the formation of the honeycomb-like electrodes by the RC regime clearly indicates the improvement of the structural stability of these electrodes in relation to the one obtained by other regimes of electrolysis, such as the PC regime and the constant galvanostatic one. 1113 1114 1115 1116 1117 1118 1119 1120 1121 1122 1123 1124 1125 1126 1127 1128 1129 1130 1131 1132 1133 1134 1135 1136 1137 1138

1139 Some of the advantages of the production of the honeycomb-like
1140 electrodes by the RC regime in relation to the constant galvanostatic
1141 and PC regimes are both the increase of the specific surface area and
1142 the improvement of their structural stability. It is clear that these
1143 advantages make this regime superior in relation to other regimes of
1144 electrolysis.

1145 **4.8 Comparison of Open Porous Copper** 1146 **Structures Obtained by Different** 1147 **Current Regimes of Electrolysis**

1148 Using the well-known fact that electrodeposition of metal by the PC
1149 and RC regimes in the millisecond range occurs at the average
1150 current density [34, 35], the formation of open porous copper
1151 structures by these regimes of electrolysis at the same average current
1152 density is examined. The obtained surface morphologies were com-
1153 pared with the one obtained in galvanostatic regime at the current
1154 density which was equal to the selected average current density.
1155 In all experiments for which results are presented here, copper
1156 electrodeposition was performed from 0.15 M CuSO_4 in 0.50 M
1157 H_2SO_4 at room temperature using cylindrical copper wires as work-
1158 ing electrodes [53]. In all PC and RC experiments, the cathodic
1159 current density of 0.44 A/cm^2 and a deposition pulse of 10 ms were
1160 selected. The average current density, j_{av} , of 0.12 A/cm^2 was reached
1161 by a selection of pause duration of 26.6 ms [for the PC regime; see
1162 Eq. (4.3)], as well as by the regulation of ratios between the anodic
1163 current density j_a and the anodic pulse duration t_a [for the RC
1164 regimes; see Eq. (4.21)]. Then, the following j_a and t_a values were
1165 selected:

- 1166 (a) $j_a = 0.040 \text{ A/cm}^2$; $t_a = 20 \text{ ms}$ (denoted as RC40)
1167 (b) $j_a = 0.20 \text{ A/cm}^2$; $t_a = 10 \text{ ms}$ (denoted as RC200)
1168 (c) $j_a = 0.52 \text{ A/cm}^2$; $t_a = 5 \text{ ms}$ (denoted RC520)

1169 Figure 4.31 shows the morphologies of electrodeposited copper
1170 obtained by the RC regimes (RC40—Fig. 4.31a; RC200—Fig. 4.31b;

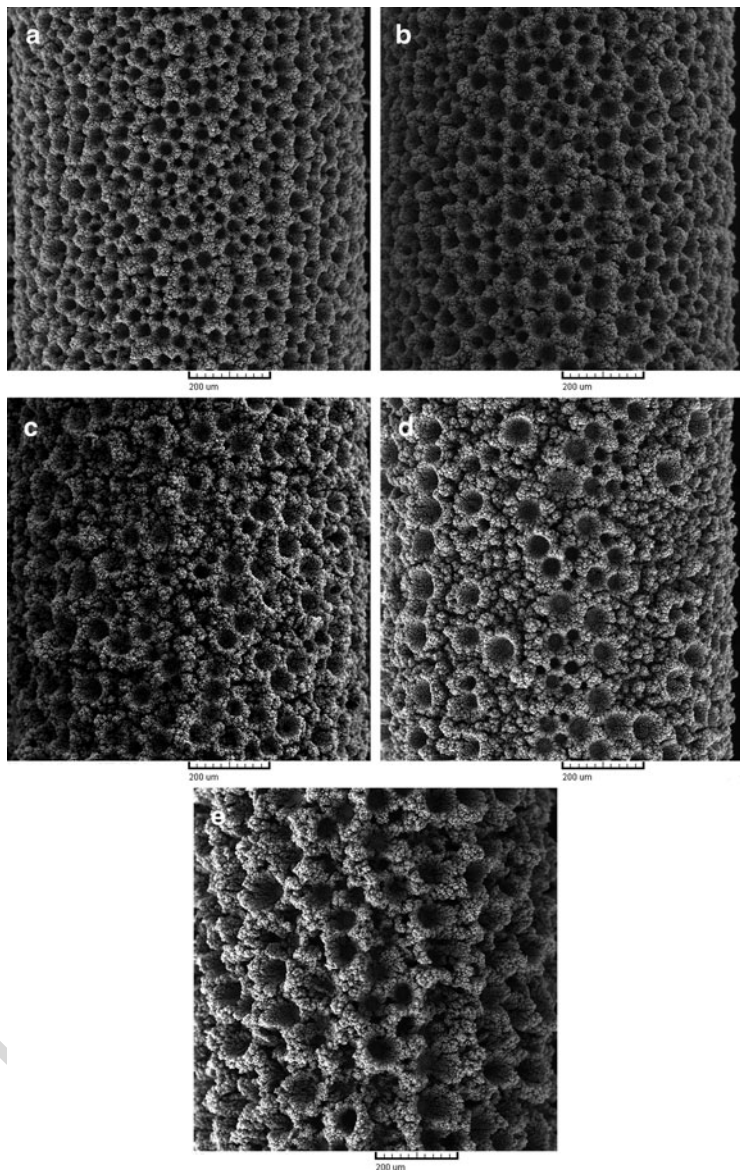


Fig. 4.31 Copper deposits obtained by: (a) RC40; (b) RC200; (c) RC520 regimes; (d) PC regime; and (e) the galvanostatic regime

1171 and RC520—Fig. 4.31c), by the PC regime (PC—Fig. 4.31d); and in
1172 the constant galvanostatic regime (DC—Fig. 4.31e). As already
1173 mentioned, the average current density was the same in all analyzed
1174 PC and RC regimes, while the applied current density in the DC
1175 mode corresponded to the average current density in the PC and RC
1176 regimes. From Fig. 4.31, it can be seen that holes formed of detached
1177 hydrogen bubbles and cauliflower-like agglomerates of copper grains
1178 or dendrites were formed under these electrodeposition conditions.
1179 These copper deposits were formed by approximately the same
1180 quantity of evolved hydrogen which corresponded to $\eta_{I,av}(H_2)$
1181 of $22.0 \pm 0.8\%$ [53]. It was understandable due to the fact that
1182 electrodeposition processes in the millisecond range at periodically
1183 changing rate occur at the average current density [34, 35].

1184 The obtained surface morphologies can be classified into two
1185 groups. In the first group are the honeycomb-like structures obtained
1186 by the RC regimes, denoted as RC40 (Fig. 4.31a) and RC200
1187 (Fig. 4.31b), as well as in the DC mode (Fig. 4.31e). The characteristic
1188 of the second group of the obtained copper deposits is the dominant
1189 presence of dish-like holes and independently formed cauliflower-like
1190 agglomerates of copper grains. These morphological forms were
1191 obtained by the RC520 (Fig. 4.31c) and PC (Fig. 4.31d) regimes.

1192 From Fig. 4.31a, b, e, it can be seen a clear difference in the size
1193 and number of holes, as well as in the wall width among them in the
1194 honeycomb-like structures obtained by the RC40 and RC200 regimes
1195 and those obtained at a constant current density. The typical holes
1196 obtained by the RC40 and the DC mode are shown in Fig. 4.32a, b,
1197 respectively. The holes obtained by the RC40 and RC200 regimes
1198 were about twice smaller than those obtained at the constant current
1199 density. The average size of these holes was about 50 μm , while holes
1200 obtained in the DC mode were about 100 μm . Morphologies of
1201 deposits among holes obtained by the RC40 regime and the DC
1202 mode are shown in Fig. 4.32c, d, respectively. The cauliflower-like
1203 agglomerates of copper grains with small dendrites on them were
1204 formed by the RC40 (Fig. 4.32c) and RC200 regimes. The nucleation
1205 exclusion zones can be clearly observed around these cauliflower-
1206 like agglomerates of copper grains. On the other hand, the relatively
1207 large cauliflower-like copper grains agglomerates surrounded by

deep irregular channels for which the origin is of evolved hydrogen were formed in the DC mode (Fig. 4.32d). Anyway, it is clear that the application of appropriate RC regime led to the redistribution of evolved hydrogen favoring growth of hydrogen bubbles with electrolysis time and hence decreasing the contribution of generated hydrogen to the creating of channel structure through the interior of the deposit (the current density distribution effect).

Dish-like holes were the dominant type of holes obtained by the PC and RC520 regimes. The typical dish-like hole obtained by the PC regime is given in Fig. 4.32e. The average diameter of this type of holes was about 100 μm . The cauliflower-like agglomerates of copper grains, and the mixture of cauliflower-like copper grains agglomerates and dendrites were formed by the PC and RC520 regimes, respectively. The typical independently formed cauliflower-like agglomerate of copper grains obtained by the PC regime is presented in Fig. 4.32f.

From technological point of view, the first group of copper deposits (the honeycomb-like structures) is especially important for the application as electrodes in electrochemical devices [1] and in catalysis [3]. It is shown that the size of holes and wall width among holes were decreased, while the number of holes was increased when the appropriate RC parameters were applied (RC40 and RC200). In this way, the specific surface of the honeycomb-like electrodes was considerably increased confirming superiority the regime of reversing current in relation to other current regimes of electrolysis (the PC regime and the constant galvanostatic regime).

Comparing all periodically changing regimes of electrolysis, it can be noticed that the effects attained by the application of the RC regimes on microstructural characteristics of the honeycomb-like structures were more similar to those attained by the regime of pulsating overpotential (PO) than those attained by the pulsating current (PC) regime. It was understandable due to the existence of anodic current during "off period" in the PO regimes [37].

Anyway, from the point of view of the formation of the honeycomb-like electrodes by the electrodeposition techniques, the regime of reversing current is more suitable than other current regimes of electrolysis.

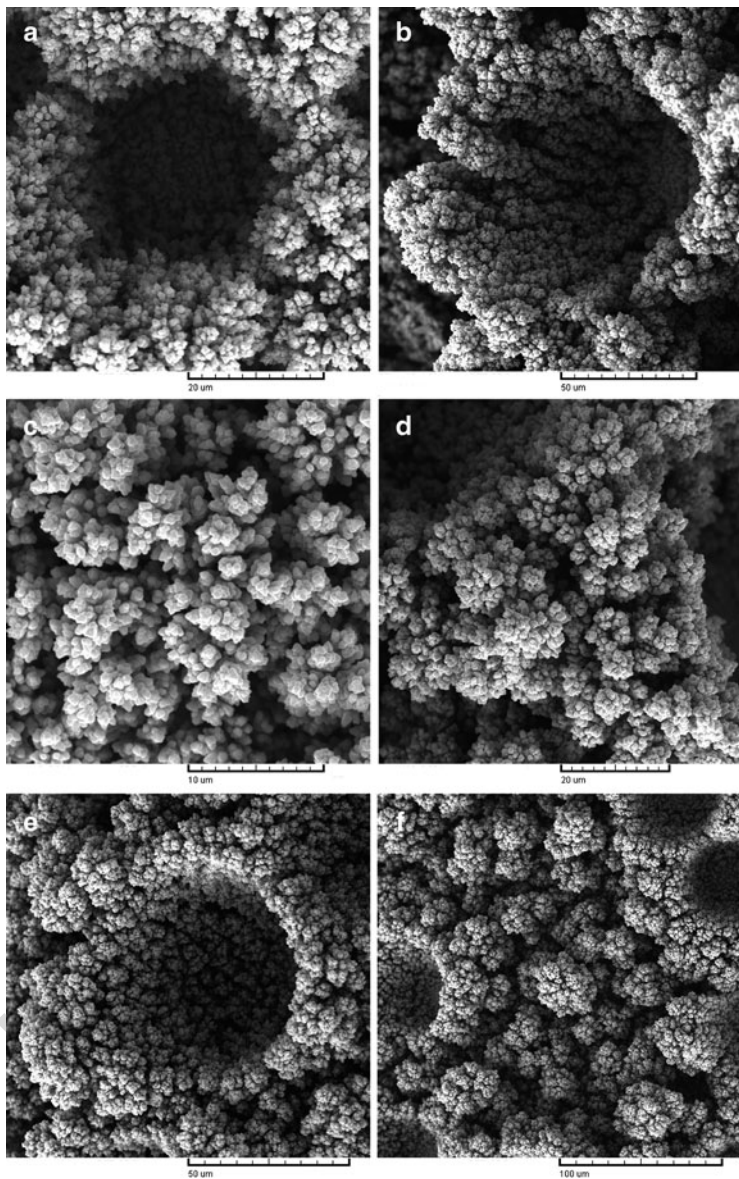


Fig. 4.32 The typical holes obtained by (a) RC40, (b) galvanostatic, and (e) PC regimes and morphological forms obtained among holes by (c) RC40, (d) galvanostatic, and (f) PC regimes

4.9 Conclusions

1245

The comprehensive survey of the formation of open porous copper structures by both the constant and periodically changing regimes of electrolysis is presented. The main characteristics of this structure type, denoted as the honeycomb-like or the 3D foam ones, are holes or pores formed of detached hydrogen bubbles surrounded by cauliflower-like agglomerates of copper grains or dendrites. In the constant regimes of electrolysis, these structures are formed at overpotentials outside the plateau of the limiting diffusion current density (the potentiostatic regime) or current densities higher than the limiting diffusion current density (the galvanostatic regime), where parallel to copper electrodeposition hydrogen evolution reaction occurs. The number, size, and distribution of holes in the honeycomb-like structures depended on the Cu(II) ions and H₂SO₄ concentrations, temperature of electrolysis, the type of the working electrode used, and a time of electrolysis.

In periodically changing regimes of electrolysis, such as the pulsating overpotential (PO), the pulsating current (PC), and the reversing current (RC) regimes, the overpotential amplitude (in the PO regime), the current density amplitude (in the PC regime), or the cathodic current density (in the RC regime) is outside (the PO regime) or higher than the limiting diffusion current density (the PC and RC regimes). The following conveniences in the production of the honeycomb-like structures can be attained since the appropriate square-waves parameters of periodically changing regimes of electrolysis are selected (a) energy saving; (b) the increase of the specific surface area of the electrodes; and (c) probably the improvement of the deposit structural stability due to the decrease of the quantity of evolved hydrogen needed for their formation.

Acknowledgments The author is grateful to Prof. Dr. Konstantin I. Popov for helpful discussion during the preparation of this chapter.

Also, the author is grateful to Dr. Goran Branković and Dr. Ljubica Pavlović for SEM analysis of investigated systems, as well as to Dr. Vesna Maksimović for the cross-section analysis of the obtained deposits.

The work was supported by the Ministry of Education and Science of the Republic of Serbia under the research project "Electrochemical synthesis and characterization of nanostructured functional materials for application in new technologies" (No. 172046).

1283 **References**

- 1284 1. Shin H-C, Dong J, Liu M (2003) *Adv Mater* 15:1610
1285 2. Shin H-C, Liu M (2005) *Adv Funct Mater* 15:582
1286 3. Yin J, Jia J, Zhu L (2008) *Int J Hydrogen Energy* 33:7444
1287 4. Shin H-C, Liu M (2004) *Chem Mater* 16:5460
1288 5. Li Y, Jia W-Z, Song Y-Y, Xia XH (2007) *Chem Mater* 19:5758
1289 6. Guo YL, Yui H, Minamikawa H, Yang B, Masuda M, Ito K, Shimizu T (2006)
1290 *Chem Mater* 18:1577
1291 7. Kazeminezhad I, Barnes AC, Holbrey JD, Seddon KR, Schwarzacher W
1292 (2007) *Appl Phys A Mater Sci Process* 86:373
1293 8. Yuan JH, He FY, Sun DC, Xia XH (2004) *Chem Mater* 16:1841
1294 9. Yuan JH, Wang K, Xia XH (2005) *Adv Funct Mater* 15:803
1295 10. Qiu JD, Peng HZ, Liang RP, Li J, Xia XH (2007) *Langmuir* 23:2133
1296 11. Wang CH, Yang C, Song YY, Gao W, Xia XH (2005) *Adv Funct Mater*
1297 15:1267
1298 12. Chen W, Xia XH (2007) *Chemphyschem* 8:1009
1299 13. Meldrum FC, Seshadri R (2000) *Chem Commun* 1:29
1300 14. Bartlett PN, Birkin PR, Ghanem MA, Toh C-S (2001) *J Mater Chem* 11:849
1301 15. Briseno AL, Han S, Rauda IE, Zhou F, Toh C-S, Nemanick EJ, Lewis NS
1302 (2004) *Langmuir* 20:219
1303 16. Nikolić ND, Popov KI, Pavlović LjJ, Pavlović MG (2006) *J Electroanal*
1304 *Chem* 588:88
1305 17. Nikolić ND, Popov KI, Pavlović LjJ, Pavlović MG (2006) *Surf Coat Technol*
1306 201:560
1307 18. Nikolić ND, Popov KI, Pavlović LjJ, Pavlović MG (2007) *J Solid State*
1308 *Electrochem* 11:667
1309 19. Nikolić ND, Pavlović LjJ, Pavlović MG, Popov KI (2007) *Electrochim Acta*
1310 52:8096
1311 20. Nikolić ND, Popov KI, Pavlović LjJ, Pavlović MG (2007) *Sensors* 7:1
1312 21. Nikolić ND, Pavlović LjJ, Krstić SB, Pavlović MG, Popov KI (2008) *Chem*
1313 *Eng Sci* 63:2824
1314 22. Nikolić ND, Branković G, Pavlović MG, Popov KI (2008) *J Electroanal*
1315 *Chem* 621:13
1316 23. Nikolić ND, Popov KI (2010) Hydrogen co-deposition effects on the structure
1317 of electrodeposited copper. In: Djokić SS (ed) *Electrodeposition: theory and*
1318 *practice*, vol 48, Modern aspects of electrochemistry. Springer, New York,
1319 pp 1–70
1320 24. Nikolić ND, Maksimović V, Pavlović MG, Popov KI (2009) *J Serb Chem Soc*
1321 74:689
1322 25. Casas JM, Alvarez F, Cifuentes L (2000) *Chem Eng Sci* 55:6223
1323 26. Nikolić ND, Pavlović LjJ, Branković G, Pavlović MG, Popov KI (2008)
1324 *J Serb Chem Soc* 73:753
1325 27. Nikolić ND, Pavlović LjJ, Pavlović MG, Popov KI (2007) *J Serb Chem Soc*
1326 72:1369

28. Amadi A, Gabe DR, Goodenough M (1991) <i>J Appl Electrochem</i> 21:1114	1327
29. Vogt H, Balzer RJ (2005) <i>Electrochim Acta</i> 50:2073	1328
30. Nikolić ND, Branković G, Popov KI (2011) <i>Mater Chem Phys</i> 125:587	1329
31. Kim J-H, Kim R-H, Kwon H-S (2008) <i>Electrochem Commun</i> 10:1148	1330
32. Oniciu L, Muresan L (1991) <i>J Appl Electrochem</i> 21:565	1331
33. Muresan L, Varvara S (2005) Leveling and brightening mechanisms in metal electrodeposition. In: Nunez M (ed) <i>Metal electrodeposition</i> . Nova Science, New York, pp 1–45	1332 1333 1334
34. Popov KI, Maksimović MD (1989) Theory of the effect of electrodeposition at periodically changing rate on the morphology of metal deposition. In: Conway BE, Bockris JO'M, White RE (eds) <i>Modern aspects of electrochemistry</i> , vol 19. Plenum, New York, pp 193–250	1335 1336 1337 1338
35. Popov KI, Djokić SS, Grgur BN (2002) <i>Fundamental aspects of electrometallurgy</i> . Kluwer Academic/Plenum, New York	1339 1340
36. Nikolić ND, Branković G, Pavlović MG, Popov KI (2009) <i>Electrochem Commun</i> 11:421	1341 1342
37. Nikolić ND, Branković G, Maksimović VM, Pavlović MG, Popov KI (2010) <i>J Solid State Electrochem</i> 14:331	1343 1344
38. Popov KI, Nikolić ND, Živković PM, Branković G (2010) <i>Electrochim Acta</i> 55:1919	1345 1346
39. Popov KI, Stojilković ER, Radmilović V, Pavlović MG (1997) <i>Powder Technol</i> 93:55	1347 1348
40. Barton L, Bockris JO'M (1962) <i>Proc R Soc A</i> 268:485	1349
41. Nikolić ND, Branković G, Maksimović VM, Pavlović MG, Popov KI (2009) <i>J Electroanal Chem</i> 635:111	1350 1351
42. Ko W-Y, Chen W-H, Tzeng S-D, Gwo S, Lin K-J (2006) <i>Chem Mater</i> 18:6097	1352 1353
43. Popov KI, Pavlović MG (1993) Electrodeposition of metal powders with controlled grain size and morphology. In: White RE, Bockris JOM, Conway BE (eds) <i>Modern aspects of electrochemistry</i> , vol 24. Plenum, New York, pp 299–391	1354 1355 1356 1357
44. Nikolić ND, Branković G, Maksimović V. <i>J Solid State Electrochem</i> . doi: 10.1007/s10008-011-1331-x	1358 1359
45. Nikolić ND, Branković G (2010) <i>Electrochem Commun</i> 12:740	1360
46. Dima GE, de Vooy's ACA, Koper MTM (2003) <i>J Electroanal Chem</i> 554–555:15	1361 1362
47. Ko W-Y, Chen W-H, Cheng C-Y, Lin K-J (2009) <i>Sens Actuators B Chem</i> 137:437	1363 1364
48. Pletcher D, Poorbedi Z (1979) <i>Electrochim Acta</i> 24:1253	1365
49. Gorgievski M, Božić D, Stanković V, Bogdanović G (2009) <i>J Hazard Mater</i> 170:716	1366 1367
50. Chandrasekar MS, Pushpavanam M (2008) <i>Electrochim Acta</i> 53:3313	1368
51. Sun BK, O'keefe TJ (1998) <i>Surf Coat Technol</i> 106:44	1369
52. Nikolić ND, Branković G, Maksimović VM. <i>J Electroanal Chem</i> (in press)	1370
53. Nikolić ND, Branković G, to be published	1371